Quantum states and optical responses of low-dimensional electron–hole systems

2004 J. Phys.: Condens. Matter 16 S3567

(http://iopscience.iop.org/0953-8984/16/35/002)

INSTITUTE OF PHYSICS PUBLISHING JOURNAL OF PHYSICS: CONDENSED MATTER

J. Phys.: Condens. Matter **16** (2004) S3567–S3595 PII: S0953-8984(04)83323-X

Quantum states and optical responses of low-dimensional electron–hole systems

Tetsuo Ogawa

Department of Physics, Osaka University, and CREST, JST, Toyonaka, Osaka 560-0043, Japan

E-mail: ogawa@mailaps.org

Received 6 July 2004
Published 20 August 2004
Online at stacks.iop.org/JPhysCM/16/S3567
doi:10.1088/0953-8984/16/35/002

Abstract

Quantum states and their optical responses of low-dimensional electron–hole systems in photoexcited semiconductors and/or metals are reviewed from a theoretical viewpoint, stressing the electron–hole Coulomb interaction, the excitonic effects, the Fermi-surface effects and the dimensionality. Recent progress of theoretical studies is stressed and important problems to be solved are introduced. We cover not only single-exciton problems but also few-exciton and many-exciton problems, including electron–hole plasma situations. Dimensionality of the Wannier exciton is clarified in terms of its linear and nonlinear responses. We also discuss a biexciton system, exciton bosonization technique, high-density degenerate electron–hole systems, gas–liquid phase separation in an excited state and the Fermi-edge singularity due to a Mahan exciton in a low-dimensional metal.

1. Introduction

Stimulated by recent progress in fabrication techniques of low-dimensional semiconductors, geometrical confinement effects on their transport and optical properties have been attracting much attention. In particular, optical characteristics of such materials, which reflect higher excited states and the relaxation effects, are of special importance in terms of not only fundamental condensed-matter physics [1] but also photonic device applications. In linear optical responses of semiconductors or insulators, an electron and a hole excited, respectively, in a conduction and a valence band, or their composite particle called an exciton, play central roles. In low-dimensional structures, the Coulomb correlation effects or the excitonic effects become more prominent than in bulk structures, leading to peculiar optical characteristics combined with geometrical confinement effects. In this paper, quantum states and their optical responses of low-dimensional photoexcited semiconductors are reviewed from a theoretical viewpoint, stressing the electron–hole Coulomb interaction and the excitonic

effects. Recent progress of theoretical studies is highlighted and important problems to be solved are introduced.

This paper is organized as follows. In section 2, fundamental remarks on low-dimensional electron–hole systems are summarized. Section 3 is devoted to single-exciton problems, including linear and nonlinear optical responses of the Wannier exciton in low dimensions. Nonlinear optical quantities (e.g., two-photon absorption rates) are stressed in terms of a probe for determining the exciton's dimensionality. In section 4, an excitonic molecule in one dimension is analysed numerically. Several treatments for the exciton–exciton correlation are introduced in section 5 to clarify an origin of $\chi^{(3)}$ excitonic nonlinearities in terms of the fermionic or bosonic picture. Deviation of an exciton from a pure boson (i.e. anharmonicity and the exciton–exciton interaction) is of importance in four-wave-mixing processes. In section 6, quantum order of a one-dimensional high-density electron–hole system at zero temperature is analytically clarified with the use of the two-band Tomonaga–Luttinger model. Section 7 is used to discuss the dynamics of the gas–liquid phase separation in an excited state at finite temperature. How the finite lifetime of the particles affects the spinodal decomposition is clarified. The dynamical responses of one-dimensional metals are reviewed in section 8, where a Mahan exciton and the Fermi-edge singularity (FES) are introduced. Recent progress of the FES theory in one and two dimensions is given in section 9, where we show that the FES is crucially affected by the trion (charged exciton complex) configuration as well as the Mahan exciton.

2. Remarks on low-dimensional electron–hole systems

When we define an exciton as a bound state of an electron in a conduction band and a hole in a valence band[1], there are two limiting types of exciton: the Wannier exciton and the Frenkel exciton. Generally speaking, the wavefunction of the electron–hole relative motion of the Wannier exciton is more sensitively affected by a spatial geometry than that of the Frenkel excitons. Thus we will review theoretical problems related to the electron–hole relative motion of a Wannier exciton confined in $d = 1$ [2] or $d = 2$.

The Wannier exciton has three degrees of freedom: a centre-of-mass motion, an electron–hole relative motion and a spin configuration, where the latter two are internal degrees of freedom. In perfect rigid crystals in d dimensions ($d = 1, 2, 3$), the centre-of-mass motion is well described by a plane wave with a d-dimensional wavevector $\boldsymbol{K}$. Since only the centre-of-mass state of $\boldsymbol{K} \sim 0$ contributes to the optical responses, the electron–hole relative motion and the subband (sublevel) structures mainly determine the optical properties of low-dimensional exciton systems. In the following, we consider a quasi-two-dimensional ($d \simeq 2$) and a quasi-one-dimensional ($d \simeq 1$) semiconductor[2] with a dipole-allowed direct band gap $E_{\rm gap}^{(d)}$,[3] which consists of a single conduction band and a single valence band [3].

The relation between the number of excitons[4] and the optical responses is a long-standing problem in exciton physics. Under a weak excitation condition, only an electron and a hole are created, which form a bound state due to the Coulomb attraction. This is just a two-

[1] Although an exciton in the narrow sense means only the lowest-energy (1s) state in electron–hole bound states, there exist many bound states in general. In the broad sense, scattering (unbound) states of an electron and a hole are also treated as excitons.

[2] Dimensionality of the electron–hole relative motion will be defined afterwards. In this paper, the 'quasi-two-dimensional' ('quasi-one-dimensional') case with a finite confinement width of the system is denoted as '$d \simeq 2$' ('$d \simeq 1$'). The purely two-dimensional (one-dimensional) case is written as $d = 2$ ($d = 1$).

[3] The upward energy shift due to the subband formation is included in the definition of $E_{\rm gap}^{(d)}$.

[4] We should note that the number of excitons is not always a well-defined quantity. Fluctuation of the exciton number is often important.

body problem, which can be solved in principle, e.g., with the use of the effective-mass approximation. However, in the case of stronger excitation where many (more than one) electrons and holes are excited in semiconductors, many-body effects should be taken into account: for example, formation of an excitonic molecule as a four-fermion problem or the Bose–Einstein condensation of excitons as a $(N + N)$-fermion problem. In any case, the interparticle Coulomb interaction plays an essential role in exciton problems.

There are several length scales characterizing the electron–hole system: the de Broglie wavelength of Bloch electrons λ_e and λ_h, the exciton effective Bohr radius a_B^* for single exciton systems in $d = 3$, the Fermi wavelength $2\pi/k_F$ for high-density degenerate electron–hole systems, the coherence/localization length of the centre-of-mass motion in unperfect crystals, and so on. The dimensionality of exciton systems depends on the ratio of the geometrical-confinement length $L_\perp$ to these length scales in which we are interested[5]. We should always bear in mind which degree of freedom is confined geometrically.

Here we note general characteristics of low-dimensional systems.

(a) The low-dimensional systems are sensitive to lattice distortions and fluctuations, which lead to the Peierls instability, self-trapped states and polaron formation. Soliton excitations are also possible in $d = 1$.
(b) Quantum fluctuation plays an important role at low temperature, which suppresses any long-range orderings. Then the mean-field approximation becomes invalid.
(c) Electronic correlation becomes of more importance due to effective reduction of the kinetic energy.
(d) The electronic structures are easily affected by the randomness. An electron or an exciton suffers from the Anderson localization in the presence of infinitesimally weak randomness.

All these features should be taken into account in general in the study of low-dimensional systems.

3. Low-dimensional Wannier exciton

To simplify the problem, we employ the effective-mass approximation and the envelope function approximation. Exchange and spin–orbit interactions are neglected here, then only the spin-singlet exciton is considered. We take the $\boldsymbol{r}_\parallel$ axis along the unconfined directions and the $\boldsymbol{r}_\perp$ axis along the confined directions. In $d \simeq 2$ systems, $\boldsymbol{r}_\parallel = (x, y)$ and $\boldsymbol{r}_\perp = z$, while for $d \simeq 1$ systems, $\boldsymbol{r}_\parallel = x$ and $\boldsymbol{r}_\perp = (y, z)$. A normalization length along the unconfined directions is $L_\parallel$. Since we are most interested in low dimensionality of the electron–hole relative motion of a Wannier exciton, $a < L_\perp < a_B^*$ is assumed[6] with the lattice constant a.

The d-dimensional exciton envelope function for $\boldsymbol{K} \sim 0$ can be written as

$$L_\parallel^{-d/2} \Psi^{(d)}_{\nu,\{\alpha\}\{\beta\}}(\boldsymbol{r}_{eh})\, \phi_{\{\alpha\}}(\boldsymbol{r}_{e\perp})\, \phi^*_{\{\beta\}}(\boldsymbol{r}_{h\perp}), \tag{1}$$

where $\boldsymbol{r}_{eh} \equiv \boldsymbol{r}_{e\parallel} - \boldsymbol{r}_{h\parallel}$ is the electron–hole relative coordinate, $\Psi^{(d)}_{\nu,\{\alpha\}\{\beta\}}$ represents the electron–hole relative motion along the unconfined ($\boldsymbol{r}_{eh}$) directions, which is specified by a quantum number(s) ν, and $\phi_{\{\alpha\}}$ ($\phi_{\{\beta\}}$) denotes a subband envelope function in the conduction (valence)

[5] An energy scale describing the geometrical confinement corresponds to the subband separation, being proportional approximately to $L_\perp^{-2}$.
[6] In the $d = 2$ limit, the exciton Bohr radius becomes $\frac{1}{2}a_B^*$. Therefore, strictly speaking, $L_\perp < \frac{1}{2}a_B^*$ is required to realize the $d \simeq 1$ situation.

band, which is determined by the shape of the confinement potential in quantum structures. When the confinement is strong, $\Psi^{(d)}_{\nu,\{\alpha\}\{\beta\}}$ satisfies

$$\left[-\frac{\hbar^2}{2\mu}\triangle_d + V^{(d)}(\boldsymbol{r}_{\rm eh})\right]\Psi^{(d)}_{\nu,\{\alpha\}\{\beta\}}(\boldsymbol{r}_{\rm eh}) = E^{(d)}_{\nu}\Psi^{(d)}_{\nu,\{\alpha\}\{\beta\}}(\boldsymbol{r}_{\rm eh}), \tag{2}$$

where μ is the electron–hole reduced mass, $\triangle_d$, d-dimensional Laplacian, $E^{(d)}_{\nu}$, an exciton energy measured from $E^{(d)}_{\rm gap}$, $V^{(d)}(\boldsymbol{r}_{\rm eh})$ the effective d-dimensional Coulomb potential,

$$V^{(d)}(\boldsymbol{r}_{\rm eh}) = \int V^{(3)}(\boldsymbol{r}_{\rm e},\boldsymbol{r}_{\rm h})|\phi_{\{\alpha\}}(\boldsymbol{r}_{\rm e\perp})|^2|\phi_{\{\beta\}}(\boldsymbol{r}_{\rm h\perp})|^2\prod {\rm d}\boldsymbol{r}_{\rm e\perp}\,{\rm d}\boldsymbol{r}_{\rm h\perp}, \tag{3}$$

with the Coulomb potential $V^{(3)}(\boldsymbol{r}_{\rm e},\boldsymbol{r}_{\rm h}) = -(e^2/\epsilon)|\boldsymbol{r}_{\rm e}-\boldsymbol{r}_{\rm h}|^{-1}$ in $d=3$, where ϵ is the relevant dielectric constant. The exciton has discrete spectra for $E^{(d)}_{\nu}<0$ and continuous spectra for $E^{(d)}_{\nu}>0$. For $d=2$ with $L_\perp\to 0$, single-exciton problems have been solved exactly [4], showing that the exciton binding energy $|E^{(2)}_0|$ is four times larger than that in $d=3$ (correspondingly, the Bohr radius becomes half). Thus the two dimensionality enhances the excitonic effects. In the $d\simeq 2$ case ($L_\perp>0$), variational approximation has been employed to discuss the excitonic effects [5].

In $d=1$ ($L_\perp\to 0$), the Coulomb attractive interaction is given by $V^{(1)}(\boldsymbol{r}_{\rm eh}) = -(e^2/\epsilon)|x_{\rm e}-x_{\rm h}|^{-1}$. Under this situation the exciton bound states have pathological features [6]:

(i) the divergence of the binding energy of the lowest state ($|E^{(1)}_0|\to\infty$),
(ii) the $\sqrt{\delta(\boldsymbol{r}_{\rm eh})}$-like wavefunction of the lowest state, and
(iii) the violation of the nondegeneracy theorem for other bound states.

These unphysical anomalies result from the divergence of the Coulomb potential at the origin ($\boldsymbol{r}_{\rm eh}=0$). Since in $d=1$ an electron and a hole cannot move without touching with each other, the divergence at the origin becomes more crucial than in higher dimensions.

In order to avoid the divergence and to obtain analytical solutions, a regularized potential [7, 8] is often employed: $V^{(1)}(\boldsymbol{r}_{\rm eh};x_0)\equiv -(e^2/\epsilon)(|\boldsymbol{r}_{\rm eh}|+x_0)^{-1}$ with a cutoff $x_0\geqslant 0$. The cutoff x_0 is found to be proportional to the lateral size of the wire (e.g., $x_0\simeq 0.18L_\perp$ for a square cross-section). Then we have relative wavefunctions of the bound states as [9]

$$\Psi^{(1)}_{\nu,\{\alpha\}\{\beta\}}(\tilde{\boldsymbol{r}}_{\rm eh}) = N_\nu\tilde{\boldsymbol{r}}_{\rm eh}{\rm e}^{-\tilde{r}_{\rm eh}/2}\Gamma(1+\nu)[F(1-\nu,2;\tilde{\boldsymbol{r}}_{\rm eh}) - G(1-\nu,2;\tilde{\boldsymbol{r}}_{\rm eh})], \tag{4}$$

where $\tilde{\boldsymbol{r}}_{\rm eh} = 2(|\boldsymbol{r}_{\rm eh}|+x_0)/(\nu a^*_{\rm B})$, N_ν is the normalization constant, $\Gamma(z)$ is the gamma function, $F(\alpha,\gamma;\tilde{\boldsymbol{r}}_{\rm eh})$ and $G(\alpha,\gamma;\tilde{\boldsymbol{r}}_{\rm eh})$ are the confluent hypergeometric functions. Here ν specifies the energy eigenvalues ($E^{(1)}_\nu = -E^*_{\rm R}/\nu^2$), which is not necessarily an integer and is determined by the additional constraints [9]:

$$\Psi^{(1)}_{\nu,\{\alpha\}\{\beta\}}(\tilde{\boldsymbol{r}}_{\rm eh}=2x_0/\nu a^*_{\rm B}) = 0 \qquad \text{(even parity state)}, \tag{5}$$

$$\left.\frac{{\rm d}\Psi^{(1)}_{\nu,\{\alpha\}\{\beta\}}(\tilde{\boldsymbol{r}}_{\rm eh})}{{\rm d}\tilde{\boldsymbol{r}}_{\rm eh}}\right|_{\tilde{r}_{\rm eh}=2x_0/\nu a^*_{\rm B}} = 0 \qquad \text{(odd parity state)}. \tag{6}$$

$E^*_{\rm R}$ is the effective Rydberg. As $x_0\to 0$ (i.e. $L_\perp\to 0$), the energy of the lowest state $E^{(1)}_0$ becomes negatively infinite, indicating the divergence of the binding energy. This is a peculiar feature of the $d=1$ exciton. When $x_0=0$, other bound states become doubly degenerate for odd and even parities at finite energies, $-E^*_{\rm R}(n-1)^{-2}$ with $n=2,3,4,\ldots$. These features suggest that the attractive force between an electron and a hole in $d\simeq 1$ systems is more effective than in $d\simeq 2$ systems [10].

Because the above results are based on the continuum model with the effective-mass and the envelope-function approximations, the ultraviolet cutoff or the finiteness of the lattice

Table 1. The subband selection rules in the one-photon-absorption (OPA) process for the arbitrary polarization direction $\hat{\varepsilon}$ of the incident light.

Exciton dimension, d	Arbitrary $\hat{\varepsilon}$
$\simeq 2$	$\alpha_z - \beta_z = \text{even} \simeq 0$
$\simeq 1$	$\alpha_y - \beta_y = \text{even} \simeq 0$ and $\alpha_z - \beta_z = \text{even} \simeq 0$

constant is not taken into account. Nevertheless, enhancement of the excitonic effects is obvious in lower dimensions.

3.1. One-photon absorption process

The transition probability between the ground state and an exciton state is reflected in the one-photon absorption (OPA) spectrum. The OPA coefficient of the d-dimensional exciton is proportional to

$$W_{\mathrm{OPA}}^{(d)}(\omega) \propto |\langle c|\hat{\varepsilon}\cdot\boldsymbol{p}|v\rangle|^2 \sum_{\{\alpha\}}\sum_{\{\beta\}} |\langle\phi_{\{\alpha\}}|\phi_{\{\beta\}}\rangle|^2 \sum_{\nu} |\Psi^{(d)}_{\nu,\{\alpha\}\{\beta\}}(\boldsymbol{r}_{\mathrm{eh}}=0)|^2 \times \delta(\hbar\omega - E^{(d)}_{\mathrm{gap}} - E^{(d)}_{\nu}), \tag{7}$$

where $\langle c|\hat{\varepsilon}\cdot\boldsymbol{p}|v\rangle$ is the interband-transition dipole matrix element with polarization unit-vector $\hat{\varepsilon}$ and momentum operator $\boldsymbol{p}$, and $|c\rangle$ ($|v\rangle$) is the band wavefunction. Here we assume for $d \simeq 1$ that $\phi_{\{\alpha\}}$ and $\phi_{\{\beta\}}$ have decoupled forms such as $\phi_{\{\alpha\}} \simeq \prod_{i=y,z}\phi_{\alpha_i}(i)$. From this, the subband selection rules become $\alpha_z - \beta_z = \text{even} \simeq 0$ for $d \simeq 2$, and $\alpha_y - \beta_y = \text{even} \simeq 0$ and $\alpha_z - \beta_z = \text{even} \simeq 0$ for $d \simeq 1$, as summarized in table 1.

The one-photon transition is allowed only for the exciton bound states with an even parity, $|\Psi^{(d)}_{\nu,\{\alpha\}\{\beta\}}(\boldsymbol{r}_{\mathrm{eh}}=0)| \neq 0$ (e.g., the 1s state). The bound states with an odd parity ($|\Psi^{(d)}_{\nu,\{\alpha\}\{\beta\}}(\boldsymbol{r}_{\mathrm{eh}}=0)| = 0$, e.g., the 2p state) are not reflected in OPA at all. The oscillator strength ($f^{(d)}_{\nu,\{\alpha\}\{\beta\}} \propto |\Psi^{(d)}_{\nu,\{\alpha\}\{\beta\}}(\boldsymbol{r}_{\mathrm{eh}}=0)|^2$) of the lowest-energy bound state (always even parity) becomes anomalously large. The oscillator strength of other bound states with an even parity vanishes completely in the limit of $x_0 \to 0$. Thus, in $d \simeq 1$ the OPA of only the lowest exciton state is extremely (divergingly) strong in comparison with the other bound states [11, 12].

Above the band-gap energy ($\hbar\omega \geqslant E^{(d)}_{\mathrm{gap}}$), the difference in the interband OPAs in $d \simeq 2$ and $d \simeq 1$ excitons is more clear[7]. For the $d \simeq 2$ systems, the interband absorption is enhanced due to excitonic effects, while it is reduced for the $d \simeq 1$ exciton systems. To see this, the Sommerfeld factor, which is defined as the ratio of the interband OPA rate with excitonic effects to that without excitonic effects, has been evaluated for $d = 2$ and $d \simeq 1$. The Sommerfeld factor for $d = 2$ is

$$S^{(2)}(\hbar\omega) = \frac{\mathrm{e}^{\pi\alpha_2}}{\cosh(\pi\alpha_2)} \geqslant 1, \tag{8}$$

where $\alpha_2 = \alpha_2(\hbar\omega) = [2\mu(a^*_{\mathrm{B}})^2(\hbar\omega - E^{(2)}_{\mathrm{gap}})]^{-1/2}$. The OPA rate at the band edge ($\hbar\omega = E^{(2)}_{\mathrm{gap}}$) is twice as large as that without the excitonic effect, i.e. $S^{(2)}(\hbar\omega = E^{(2)}_{\mathrm{gap}}) = 2$. The Sommerfeld factor for $d = 2$ is also called the Coulomb 'enhancement' factors because of $S^{(2)}(\hbar\omega) \geqslant 1$. On the other hand, the Sommerfeld factor for $d \simeq 1$ is

$$S^{(1)}(\hbar\omega; x_0) = \frac{\mathrm{e}^{\pi\alpha_1}}{8} \frac{\left|D^{(2)}_0 W^{(1)}_0 - D^{(1)}_0 W^{(2)}_0\right|^2}{|D^{(1)}_0|^2 + |D^{(2)}_0|^2} \leqslant 1, \tag{9}$$

[7] The OPA strength is proportional to the joint density of states (JDOS) when no electron–hole Coulomb interaction is taken into account.

where $\alpha_1 = \alpha_1(\hbar\omega) \equiv [2\mu(a_B^*)^2(\hbar\omega - E_{gap}^{(1)})]^{-1/2}$. Here $W_0^{(j)} \equiv W^{(j)}(\tilde{r}_{eh} = 2ikx_0)$, $D_0^{(j)} \equiv dW^{(j)}(\tilde{r}_{eh})/d\tilde{r}_{eh}|_{\tilde{r}_{eh}=2ikx_0}$, and

$$W^{(j)}(\boldsymbol{r}_{eh}) \equiv \tilde{r}_{eh}e^{-\tilde{r}_{eh}/2}\Gamma(1 \pm i\alpha_1)[F(1 + i\alpha_1, 2; \tilde{r}_{eh}) \pm G(1 + i\alpha_1, 2; \tilde{r}_{eh})], \tag{10}$$

for $j = 1$ (2) corresponding to the + (−) sign of the right-hand side. Here the scattering state of the $d \simeq 1$ exciton of energy $E_k^{(1)} = \hbar\omega > 0$ is characterized by the wavenumber k through $E_k^{(1)} = \hbar^2k^2/2\mu$. The Sommerfeld factor in $d \simeq 1$ is less than unity, which means that the electron–hole Coulomb attraction suppresses the OPA of an allowed interband transition. At $\hbar\omega = E_{gap}^{(1)}$, i.e. $\alpha_1 \to +\infty$, the Sommerfeld factor vanishes, $S^{(1)}(\hbar\omega = E_{gap}^{(1)}; x_0) = 0$, which cancels the divergence due to the joint density of states (JDOS) of $d = 1$ systems. These particular one-dimensional effects have been observed in experiments [13, 14]. In the limit of $x_0 \to 0$, *no* interband absorption takes place, i.e. $S^{(1)}(\hbar\omega; x_0 = 0) = 0$ for all $\hbar\omega \geqslant E_{gap}^{(1)}$.

3.2. Two-photon absorption process

In the OPA process, the polarization dependence appears only in the interband matrix element, $|\langle c|\hat{\varepsilon} \cdot \boldsymbol{p}|v\rangle|$. Therefore, OPA anisotropy for the polarization directions reflects only that of the Bloch (band) electrons not of the excitons nor of the subband structures. On the other hand, the two-photon absorption (TPA) process reflects directly the dimensionality of excitons, i.e. squeezing of the wavefunction of the exciton's relative motion itself in a low-dimensional geometry. We shall now discuss the polarization anisotropy of the TPA.

Consider the situation where the photon energies $\hbar\omega_1$ and $\hbar\omega_2$ of incident light beams are both close to $\frac{1}{2}E_{gap}^{(d)}$ and these two beams have a common polarization vector $\hat{\varepsilon}$. The complete summation over all the intermediate states is performed by approximating off-resonant energy denominators as a constant [15]. Contrary to the OPA case, the TPA probability $W_{TPA}^{(d)}$ for d-dimensional exciton systems has different forms depending on the polarization directions [16, 17].

When $\hat{\varepsilon} \parallel \boldsymbol{r}_\parallel$, the TPA rate is proportional to $W_{TPA}^{(d)}(\omega_1 + \omega_2; \hat{\varepsilon} \parallel \hat{\boldsymbol{r}}_\parallel) \propto |\langle c|\hat{\varepsilon} \cdot \boldsymbol{p}|v\rangle|^2\mu_\parallel^{-2}G^{(d)}(\hat{\varepsilon} \parallel \boldsymbol{r}_\parallel)$, where

$$G^{(d)}(\hat{\varepsilon} \parallel \boldsymbol{r}_\parallel) = (L_{norm})^{d-3}\sum_{\{\alpha\}}\sum_{\{\beta\}}\left|\langle\phi_{\{\alpha\}}|\phi_{\{\beta\}}\rangle\right|^2\sum_\nu\left|\frac{\partial}{\partial\boldsymbol{r}_{eh}}\Psi_{\nu,\{\alpha\}\{\beta\}}^{(d)}(\boldsymbol{r}_{eh})\right|^2_{\boldsymbol{r}_{eh}=0}$$
$$\times\,\delta(\hbar\omega_1 + \hbar\omega_2 - E_{gap}^{(d)} - E_\nu^{(d)}), \tag{11}$$

with L_{norm} the normalization length along the $\boldsymbol{r}_\perp$ direction and $\mu_\parallel$ the electron–hole reduced mass for the motion along $\boldsymbol{r}_\parallel$ direction. Here we find the subband selection rule: $\alpha_z - \beta_z =$ even $\simeq 0$ for $d \simeq 2$ and $\alpha_i - \beta_i =$ even $\simeq 0$ ($i = y$ or z) for $d \simeq 1$. These are identical with those in the OPA case. Only the odd-parity states are allowed for the TPA process of $\hat{\varepsilon} \parallel \boldsymbol{r}_\parallel$ because the derivative of the exciton wavefunction at the origin is nonzero only for odd-parity states, which are forbidden for the OPA process.

On the other hand, when $\hat{\varepsilon} \parallel \boldsymbol{r}_\perp$, the TPA coefficient is proportional to $W_{TPA}^{(d)}(\omega_1 + \omega_2; \hat{\varepsilon} \parallel \boldsymbol{r}_\perp) \propto |\langle c|\hat{\varepsilon} \cdot \boldsymbol{p}|v\rangle|^2\mu_\zeta^{-2}G^{(d)}(\hat{\varepsilon} \parallel \boldsymbol{r}_\perp)$, with

$$G^{(d)}(\hat{\varepsilon} \parallel \boldsymbol{r}_\perp) = (L_{norm})^{d-3}\sum_{\alpha_\zeta}\sum_{\beta_\zeta}\left|\langle\phi_{\alpha_\zeta}|\frac{\partial}{\partial x_\zeta}|\phi_{\beta_\zeta}\rangle\right|^2\sum_{\alpha_{\zeta'}}\sum_{\beta_{\zeta'}}|\langle\phi_{\alpha_{\zeta'}}|\phi_{\beta_{\zeta'}}\rangle|^2$$
$$\times\left|\sum_\nu\Psi_{\nu,\{\alpha\}\{\beta\}}^{(d)}(\boldsymbol{r}_{eh} = 0)\right|^2\delta(\hbar\omega_1 + \hbar\omega_2 - E_{gap}^{(d)} - E_\nu^{(d)}), \tag{12}$$

where μ_ζ is the electron–hole reduced mass for the motion along the confinement direction. For $d \simeq 1$, ζ is an index specifying a component of $\boldsymbol{r}_\perp = (y, z)$ parallel to the polarization

Table 2. The subband selection rules in the two-photon-absorption (TPA) process for a polarization direction $\hat{\varepsilon}$ of the incident lights. For $d \simeq 1$, ζ is an index specifying an component of $r_\perp = (y, z)$ parallel to the polarization direction $\hat{\varepsilon}$, while ζ' indicates the rest component in $r_\perp$.

Exciton dimension, d	$\hat{\varepsilon} \parallel r_\parallel$	$\hat{\varepsilon} \parallel r_\perp$
$\simeq 2$	$\alpha_z - \beta_z = \text{even} \simeq 0$	$\alpha_z - \beta_z = \text{odd} \simeq \pm 1$
$\simeq 1$	$\alpha_y - \beta_y = \text{even} \simeq 0$ and $\alpha_z - \beta_z = \text{even} \simeq 0$	$\alpha_\zeta - \beta_\zeta = \text{odd} \simeq \pm 1$ and $\alpha_{\zeta'} - \beta_{\zeta'} = \text{even} \simeq 0$

direction $\hat{\varepsilon}$, while ζ' indicates the rest component in $\boldsymbol{r}_\perp$. The subband selection rule for $d \simeq 2$ is $\alpha_z - \beta_z = \text{odd} \simeq \pm 1$, while for $d \simeq 1$, $\alpha_\zeta - \beta_\zeta = \text{odd} \simeq \pm 1$ for the polarization direction, and $\alpha_{\zeta'} - \beta_{\zeta'} = \text{even} \simeq 0$ for the other confinement direction. Only the even-parity states are allowed for the TPA process of $\hat{\varepsilon} \parallel \boldsymbol{r}_\perp$ because $\Psi^{(d)}_{\nu,\{\alpha\}\{\beta\}}(\boldsymbol{r}_{\text{eh}} = 0)$ is nonzero only for even-parity excitons, which are allowed for the OPA process. We find that not only even-parity states but also odd-parity ones can be detected by TPA with appropriate control of the polarization direction. These anisotropic TPA characteristics result directly from low-dimensional natures of the electron–hole relative motion. The subband selection rule is also anisotropic depending on the polarization direction, as summarized in table 2.

In the regions of continuous spectra ($\hbar\omega_1 + \hbar\omega_2 \geqslant E^{(d)}_{\text{gap}}$), the $d \simeq 1$ exciton effects enhance the TPA for $\hat{\varepsilon} \parallel \hat{x}$ (the unconfinement direction), whereas they reduce the TPA for $\hat{\varepsilon} \parallel \hat{x}_\zeta$ (the confinement direction), which is in striking contrast to the higher-dimensional cases, where the TPA is always enhanced by excitonic effects. As a result, in the case of the TPA in $d = 1$, one can observe both the reduction (for $\hat{\varepsilon} \parallel \hat{x}$) and enhancement (for $\hat{\varepsilon} \parallel \hat{x}_\zeta$) in the same sample simply by rotating the polarization direction. In an intermediate regime between $d \simeq 2$ and $d \simeq 1$, the dimensional crossover effects appear only in the TPA process (not in the OPA) [18]. These theories can explain experimental results [19, 20].

3.3. Dielectric confinement effect

In determining the effective Coulomb potential in less than two dimensions, we need to include the dielectric image-charge effect arising from the difference in the dielectric constant between the material (ϵ) and the surroundings (ϵ_1). This is a confinement effect of the Coulomb interaction. If the surrounding materials have a smaller dielectric constant and a larger energy gap than the relevant material, the electron–hole Coulomb attraction in the relevant material works very effectively through the surroundings with reduced screening. As a result, the exciton binding energy is expected to increase much more than in a normal low-dimensional system without this effect.

We shall consider a $d \simeq 2$ system with the well width $L_\perp(|z| \leqslant \frac{1}{2}L_\perp)$ (its dielectric constant is ϵ) [21, 22]. The barrier regions have the dielectric constants, ϵ_1 ($\epsilon > \epsilon_1$). The electrostatic interaction between two point charges in the $d \simeq 2$ system is given by

$$V^{(2)}_{\text{image}}(\boldsymbol{r}_{\text{eh}}) = -\frac{e^2}{\epsilon}\int \mathrm{d}^2\boldsymbol{k}\,\frac{\mathrm{e}^{\mathrm{i}\boldsymbol{k}\cdot\boldsymbol{r}_{\text{eh}}}}{k\sinh(kL_\perp + 2\eta)} \times \cosh\left[k\left(\frac{L_\perp}{2} - z_{\text{e}}\right) + \eta\right]\cosh\left[k\left(\frac{L_\perp}{2} + z_{\text{h}}\right) + \eta\right]. \tag{13}$$

Here $k = |\boldsymbol{k}| = \sqrt{k_x^2 + k_y^2}$, $\eta = \frac{1}{2}\ln[(\epsilon + \epsilon_1)/(\epsilon - \epsilon_1)]$, $\boldsymbol{r}_{\text{eh}} = (x_{\text{eh}}, y_{\text{eh}}) = (x_{\text{e}} - x_{\text{h}}, y_{\text{e}} - y_{\text{h}})$.

(i) When the electron is close to the hole ($r^2 \equiv |\boldsymbol{r}_{\text{eh}}|^2 + z^2_{\text{eh}} \ll L^2_\perp$), the interaction is identical to that in bulk.

(ii) When the electron is far from the hole ($|\boldsymbol{r}_{\rm eh}| \gg (\epsilon/\epsilon_1)L_\perp$), it is determined by ϵ_1 only, i.e. $V^{(2)}_{\rm image} \to -(e^2/\epsilon_1)|\boldsymbol{r}_{\rm eh}|^{-1}$.

(iii) When $\epsilon \gg \epsilon_1$, $V^{(2)}_{\rm image} \to -2e^2/(\epsilon L_\perp)\{\ln[(\epsilon/\epsilon_1)(L_\perp/|\boldsymbol{r}_{\rm eh}|)] - \gamma\}$ in the region of $L_\perp \ll |\boldsymbol{r}_{\rm eh}| \ll (\epsilon/\epsilon_1)L_\perp$. Here $\gamma = 0.577$.

In a square wire ($d \simeq 1$) structure ($|y| \leqslant \frac{1}{2}L_\perp$, $|z| \leqslant \frac{1}{2}L_\perp$), the electron–hole interaction including the dielectric image-charge effect is derived as [9]

$$U^{(1)}_{\rm image}(\boldsymbol{r}_{\rm e}, \boldsymbol{r}_{\rm h}) = -\frac{e^2}{\epsilon}\sum_{m=-\infty}^{\infty}\sum_{n=-\infty}^{\infty} q^{|m|+|n|}\left[x_{\rm eh}^2 + y_m^2 + z_n^2\right]^{-1/2}, \tag{14}$$

where $q \equiv (\epsilon - \epsilon_1)/(\epsilon + \epsilon_1)$, $y_m \equiv y_{\rm e} - mL_\perp - (-1)^m y_{\rm h}$, and $z_n \equiv z_{\rm e} - nL_\perp - (-1)^n z_{\rm h}$. After averaging over $y_{\rm e}$, $z_{\rm e}$, $y_{\rm h}$ and $z_{\rm h}$ on the cross-section of the wire, we have

$$V^{(1)}_{\rm image}(x_{\rm eh}) = -4E^*_{\rm R}\frac{a^*_{\rm B}}{L_\perp}\int_0^\infty {\rm d}k_y \int_0^\infty {\rm d}k_z\, F(k_y)F(k_z)\frac{\exp\left[-\pi x_{\rm eh}\sqrt{k_y^2 + k_z^2}/L_\perp\right]}{\sqrt{k_y^2 + k_z^2}}, \tag{15}$$

where

$$F(k) = \frac{1 + 2q(1-q^2)\cos(\pi k) - q^4}{1 - 2q^2\cos(2\pi k) + q^4} f(k). \tag{16}$$

Here $f(k)$ is given using $j_0(x) \equiv \sin x/x$ as

$$\begin{aligned} f(k) = {} & j_0^2\left(\frac{\pi}{2}k\right) + j_0\left(\frac{\pi}{2}(k-2)\right)j_0\left(\frac{\pi}{2}k\right) + j_0\left(\frac{\pi}{2}(k+2)\right)j_0\left(\frac{\pi}{2}k\right) \\ & + \frac{1}{4}j_0^2\left(\frac{\pi}{2}(k-2)\right) + \frac{1}{4}j_0^2\left(\frac{\pi}{2}(k+2)\right) + \frac{1}{2}j_0\left(\frac{\pi}{2}(k-2)\right)j_0\left(\frac{\pi}{2}(k+2)\right). \end{aligned} \tag{17}$$

The calculated potential with the dielectric image-charge effects $V^{(1)}_{\rm image}(x_{\rm eh})$ can be well fitted by $V^{(1)}(x_{\rm eh}; x_0)$. As the ratio ϵ/ϵ_1 increases, the attractive potential becomes more long-ranged and is enhanced for all regions of $x_{\rm eh}$ over the bare Coulomb potential $V^{(1)}(x_{\rm eh}) = -(e^2/\epsilon)|x_{\rm eh}|^{-1}$. Therefore, the peculiar features of the $d \simeq 1$ excitons would be more pronounced by the dielectric image-charge effect.

4. One-dimensional excitonic molecule

The two-exciton excited state in semiconductors is related to the excitonic molecule, which has been investigated for a long time [23]. In three dimensions, the binding energy of the excitonic molecule was shown to be always positive [24]. In this section, we shall overview theories of an excitonic molecule (EM) in $d = 1$, and the recent status of the study on excitonic nonlinearities in semiconductors is reviewed.

First, we introduce a theory of an excitonic molecule in $d \simeq 1$ with the Heitler–London approximation [8]. Here two Wannier excitons are assumed to exist in a continuum model of a $d \simeq 1$ semiconductor. The one-dimensional effective Hamiltonian is

$$\begin{aligned} \hat{H}^{(1)}_{\rm EM} = {} & -\frac{\partial^2}{\partial\xi_1^2} - \frac{\partial^2}{\partial\xi_2^2} + \frac{2\mu}{m^*_{\rm h}}\left(\frac{\partial}{\partial\xi_1} - \frac{\partial}{\partial\xi_2}\right)\frac{\partial}{\partial x_{\rm hh}} - \frac{2\mu}{m^*_{\rm h}}\frac{\partial^2}{\partial x_{\rm hh}^2} \\ & - \frac{\mu}{2(m^*_{\rm e} + m^*_{\rm h})}\frac{\partial^2}{\partial X^2} + 2U^{(1)}(\xi_1, \xi_2, x_{\rm hh}), \end{aligned} \tag{18}$$

where m_e^* (m_h^*) is the effective mass of an electron (a hole), the coordinates are defined as $\xi_1 \equiv x_{e1} - x_{h1}$, $\xi_2 \equiv x_{e2} - x_{h2}$, $x_{hh} \equiv x_{h1} - x_{h2}$, and $X \equiv [2(m_e^* + m_h^*)]^{-1}[m_e^*(x_{e1} + x_{e2}) + m_h^*(x_{h1} + x_{h2})]$, and the potential $U^{(1)}$ is given as

$$U^{(1)}(\xi_1, \xi_2, x_{hh}) = V^{(1)}(\xi_1 - \xi_2 + x_{hh}; x_0) + V^{(1)}(x_{hh}; x_0) - V^{(1)}(\xi_1; x_0) - V^{(1)}(\xi_2; x_0) - V^{(1)}(\xi_1 + x_{hh}; x_0) - V^{(1)}(\xi_2 - x_{hh}; x_0). \tag{19}$$

Here $V^{(1)}(x; x_0)$ is the regularized Coulomb potential in $d \simeq 1$. Since the polarization effect (deformation of the electron–hole relative wavefunction of an exciton due to the other exciton) is neglected, the problem of the excitonic molecule is reduced to that of the hole–hole relative motion. The binding energy of the excitonic molecule in $d \simeq 1$, $E_{EM}^{(1)}$, is given by solving the eigenvalue problem for the hole–hole relative wavefunction $\psi_{hh}^{(1)}$, i.e.

$$\left[-\frac{2\mu}{m_h^*}\frac{\partial^2}{\partial x_{hh}^2} + V_{hole}^{(1)}(x_{hh})\right]\psi_{hh}^{(1)} = -E_{EM}^{(1)}\psi_{hh}^{(1)}. \tag{20}$$

Here $V_{hole}^{(1)}(x_{hh})$ is the effective hole potential [8]:

$$V_{hole}^{(1)}(x_{hh}) = -2E_0^{(1)} + \int_{-\infty}^{\infty} d\xi_1 \int_{-\infty}^{\infty} d\xi_2\, \Phi_{corr}^{(1)}(\xi_1, \xi_2, x_{hh})\hat{H}_{EM}^{(1)}\Phi_{corr}^{(1)}(\xi_1, \xi_2, x_{hh}), \tag{21}$$

where $E_0^{(1)}$ is the ground-state exciton energy in $d \simeq 1$, and an eigenfunction of $\hat{H}_{EM}^{(1)}$ is assumed to be $\psi^{(1)}(\xi_1, \xi_2, x_{hh}) = \phi_{hh}^{(1)}(|x_{hh}|)\Phi_{corr}^{(1)}(\xi_1, \xi_2, x_{hh})$. Here $\Phi_{corr}^{(1)}$ describes the exciton correlations

$$\Phi_{corr}^{(1)}(\xi_1, \xi_2, x_{hh}) = N(x_{hh})\left[\Psi_\nu^{(1)}(\xi_1)\Psi_\nu^{(1)}(\xi_2) + \Psi_\nu^{(1)}(\xi_1 + x_{hh})\Psi_\nu^{(1)}(\xi_2 - x_{hh})\right] \tag{22}$$

with the normalization function $N(x_{hh})$, where $\Psi_\nu^{(1)}$ is the relative wavefunction of an exciton in $d \simeq 1$ given in equation (4). According to numerical calculation, $E_{EM}^{(1)}$ is more than five times larger than $E_{EM}^{(3)} \simeq 0.04E_R^*$ for bulk GaAs. Thus, an excitonic molecule becomes more stable in lower-dimensional systems, similar to the exciton case.

Conventionally, an excitonic molecule is regarded as a bound state of two (Wannier) excitons. More rigorously, however, we should solve a four-fermion problem taking into full account the correlation effect on the length scale of a lattice constant. In other words, a usual bosonic picture of the excitonic molecule cannot capture the binding mechanism quantitatively. We need to look into the way in which two electrons and two holes are reshuffled. In addition, in lower dimensions, the electronic correlation effects lead to the crossover between the Frenkel-type EM and the Wannier-type EM. In order to treat this crossover consistently, both a lattice model and the long-range interaction are required for the description of an EM. We solved the four-fermion model of an EM by exact diagonalization on a finite $d = 1$ lattice [25]. The EM Hamiltonian employed there is

$$\hat{\mathcal{H}}_{EM}^{(1)} = -t_e\sum_{i\sigma}(\hat{c}_{i+1,\sigma}^\dagger\hat{c}_{i\sigma} + \text{h.c.}) - t_h\sum_{i\sigma}(\hat{d}_{i+1,\sigma}^\dagger\hat{d}_{i\sigma} + \text{h.c.}) + E_0\sum_{i\sigma}\hat{d}_{i\sigma}^\dagger\hat{d}_{i\sigma} - \sum_{ij\sigma\sigma'}U_{ij}\,\hat{c}_{i\sigma}^\dagger\hat{c}_{i\sigma}\hat{d}_{j\sigma'}^\dagger\hat{d}_{j\sigma'} + \sum_{ij\sigma\sigma'}V_{ij}\,(\hat{c}_{i\sigma}^\dagger\hat{c}_{i\sigma}\hat{c}_{j\sigma'}^\dagger\hat{c}_{j\sigma'} + \hat{d}_{i\sigma}^\dagger\hat{d}_{i\sigma}\hat{d}_{j\sigma'}^\dagger\hat{d}_{j\sigma'}) - V_{dipole}\sum_{i\sigma}(\hat{c}_{i+1,\sigma}^\dagger\hat{d}_{i+1,-\sigma}^\dagger\hat{d}_{i,-\sigma}\hat{c}_{i\sigma} + \text{h.c.}), \tag{23}$$

where $\hat{c}_{i\sigma}^\dagger$ ($\hat{d}_{i\sigma}^\dagger$) creates an electron in the conduction band (a hole in the valence band) with spin σ at site i, t_e (t_h) is the transfer energy of electrons (holes), and E_0 is the energy difference between the two orbitals from which conduction and valence bands arise. The attractive electron–hole interaction between the sites i and j is denoted by U_{ij}, while V_{ij}

represents the repulsive electron–electron and hole–hole interactions. The last term describes the transfer of an electron–hole pair from site to site. We assumed that $U_{ij} = U_0$ for $i = j$, $U_{ij} = U_1/|i - j|$ for $i \neq j$ and $V_{ij} = V_0$ for $i = j$, $V_{ij} = V_1/|i - j|$ for $i \neq j$, where physically $U_0 > U_1 \geqslant 0$, $V_0 > V_1 \geqslant 0$ and $V_1 = U_1$.

The numerical diagonalization of the Hamiltonian has been carried out for a finite $d = 1$ system with the periodic boundary condition. We found that the Heitler–London scheme gives only about half the exact result for the whole range of the transfer energies. This discrepancy indicates that the correlation effect is of significance in $d = 1$ systems. The Heitler–London approximation is expected to give reasonable results only when the electron–hole relative motion is spatially extended. We stress, however, that in $d = 1$ systems the correlated motion of electrons and holes over the length scale of a lattice constant is essential even in the weak-coupling case. Moreover, continuum models for an EM holds only in the weak-coupling regime, where the hole–hole correlation is peaked at a finite distance larger than a lattice constant, while it decays faster for the strong-coupling regime where an EM is more compact in space and its size is of an atomic order. In $d = 1$, the coupling among particles becomes essentially stronger in comparison with that in higher dimensions. Therefore, the lattice model is suitable for description of the elementary excitations in $d = 1$ such as a $d = 1$ EM in the whole range of the electron–hole coupling constant. Other physical quantities of the $d = 1$ EM are given in [25].

In some $d \simeq 1$ materials, a novel quasiparticle called an 'excitonic n-string' [26] can be formed by n electrons and n holes with small integer n. But in general, polyexcitons of $n > 2$ become unstable in higher dimensions. 'Charged excitons' composed of two electrons and one hole (or one electron and two holes) are also predicted and observed [27]. Condensation of charge-transfer excitons is also attracting attention in terms of the photoinduced phase transitions [28, 29].

5. Optical nonlinearity due to excitonic correlations

Recently, it was recognized that the $\chi^{(3)}$ process is sensitive to details of the two-exciton state. In this section, we shall give an overview of the recent status of the study on excitonic nonlinearities in semiconductors. Nonlinear optical responses have been studied for a long time, also in relation to photonic device application and laser operation. In particular, the $\chi^{(3)}$ process is of special importance because it is the lowest-order nonlinear effect in ordinary materials. When the energy of the incident light is tuned at the 1s exciton level, the nonlinearity results from some characteristics of the 1s excitons. Relations between the $\chi^{(3)}$ nonlinearity and the interaction between the 1s excitons are investigated theoretically [30]. The aims of theoretical studies on optical nonlinearity in semiconductors is to clarify spatiotemporal dynamics of excitons (or electrons and holes) in photoexcited semiconductors and to predict temporal or spectral variations of induced nonlinear polarizations. For these purposes, there are two types of approach: the fermion-picture treatment where electrons and holes play their individual roles and the boson-picture treatment in which a pair of an electron and a hole is regarded as a composite boson.

5.1. Fermion-picture treatment

In the fermionic treatment, we start with two types of fermions considering separately electrons excited in a conduction band and holes in a valence band. The populations and the induced polarization (interband dipole moment) are traced with the Heisenberg equations of motion. A typical example of this treatment is the semiconductor Bloch equations (SEBs) [31, 32]

in momentum space. When we confine ourselves to the interband transitions neglecting intraband transitions, semiconductors are described as an ensemble of two-level atoms with inhomogeneous broadening. In analogy with the optical Bloch equations describing coherent optical transient phenomena, the equations of motion for three macroscopically averaged quantities are

$$\begin{aligned}
\frac{\mathrm{d}n_k^{\mathrm{e}}(t)}{\mathrm{d}t} &= -2\,\mathrm{Im}[\Omega_k p_k^*] - \Gamma_k^{\mathrm{e}} n_k^{\mathrm{e}},\\
\frac{\mathrm{d}n_k^{\mathrm{h}}(t)}{\mathrm{d}t} &= -2\,\mathrm{Im}[\Omega_k p_k^*] - \Gamma_k^{\mathrm{h}} n_k^{\mathrm{h}},\\
\frac{\mathrm{d}p_k(t)}{\mathrm{d}t} &= -\mathrm{i}[\tilde{\epsilon}_k^{\mathrm{e}} + \tilde{\epsilon}_k^{\mathrm{h}}]p_k - \mathrm{i}(n_k^{\mathrm{e}} + n_k^{\mathrm{h}} - 1)\Omega_k - \gamma_k p_k,
\end{aligned} \tag{24}$$

where $n_k^{\mathrm{e}}(t) \equiv \langle \sum_\sigma \hat{c}_{k\sigma}^\dagger \hat{c}_{k\sigma} \rangle$ ($n_k^{\mathrm{h}}(t) \equiv \langle \sum_\sigma \hat{d}_{k\sigma}^\dagger \hat{d}_{k\sigma} \rangle$) is the Heisenberg representation of the mean density of the conduction electrons (valence holes) with momentum $\boldsymbol{k}$ at time t and the interband polarization $p_k(t) \equiv \langle \sum_\sigma \hat{c}_{k\sigma} \hat{d}_{k\sigma} \rangle$. Here $\hat{c}_{k\sigma}^\dagger$ ($\hat{d}_{k\sigma}^\dagger$) creates an electron in the conduction band (a hole in the valence band) with momentum $\boldsymbol{k}$ and spin σ, $\tilde{\epsilon}_k^\nu \equiv \epsilon_k^\nu - \sum_q V_{|k-q|}\, n_q^\nu$ is the single-particle energy renormalized by the Coulomb interaction V_q between an electron ($\nu = \mathrm{e}$) and a hole ($\nu = \mathrm{h}$), $\Omega_k \equiv d_{cv} E(t) + \sum_{q \neq k} V_{|k-q|}\, p_q$ is the generalized Rabi frequency for the incident light field $E(t)$, d_{cv} is the interband dipole matrix element and Γ_k^ν, γ_k are the phenomenological relaxation constants.

In order to obtain a closed form of coupled equations, the Hartree–Fock (mean-field) approximation was employed, where the four (or higher) operator terms in the Heisenberg equations of motion are split into products of two-operator terms; the densities and the interband polarization. This is valid only for the case of high-density and homogeneous excitations. However, since the single exciton state of the zero centre-of-mass momentum $\boldsymbol{K} = 0$ can be described by the SBEs, it has been frequently used to analyse experimental results in bulk semiconductors even for the weak-excitation case. Nevertheless, we have to note that contribution from an excitonic molecule (two-exciton states) is completely neglected in the SBEs. This is a fatal shortcoming of this formulation for the description of the $\chi^{(3)}$ process close to the 1s exciton resonance [33, 34]. To overcome this, other fermion-picture theories, e.g., the real-space density matrix theory taking into account higher-order correlations [35] or the Green-function formalism are proposed and progressed.

5.2. Boson-picture treatment

When we consider the excitonic $\chi^{(3)}$ nonlinearity, we need to consider only the subspace containing up to two-electron excited states in the intermediate-state summation for perturbation calculations. In such a rather weak excitation regime, the screening effect is still weak, then an electron and a hole tend to make a pair (an exciton bound state) with each other. In the boson-picture treatment, a *pair* of an electron and a hole is considered as a basis, and it is treated as a (quasi)boson.

Kuwata-Gonokami *et al* carried out a degenerate four-wave mixing experiment near the 1s exciton resonance with a GaAs quantum well in a high-Q cavity under circularly polarized light irradiation. To explain their experimental results, they proposed an elastic-scattering model of two cavity polaritons [36]. The cavity polariton is a hybridized state of a 1s exciton and a photon in the cavity, and is regarded as a (quasi)boson. Such a phenomenological model is called the weakly interacting boson (WIB) model. In the WIB model, we first assume there is a pure-boson describing a quasiparticle in an excited state of the material, whose operators are written as $\hat{B}_{k\sigma}$ and $\hat{B}_{k\sigma}^\dagger$ with an internal degree of freedom (helicity or total angular

momentum) $\sigma = \pm 1$. They are assumed to satisfy the pure-boson commutation relation: $[\hat{B}_{k\sigma}, \hat{B}^{\dagger}_{k'\sigma'}] = \delta_{kk'}\delta_{\sigma\sigma'}$. Usually, this pure-boson describes a 1s exciton in an approximate sense. Only three types of interaction (whose momentum dependence is neglected) between bosons and photons are required:

(a) an attractive interaction W between bosons with different total angular momentum,
(b) a repulsive interaction R between bosons with an identical total angular momentum, and
(c) the phase-space filling effect G resulting from Pauli's exclusion principle.

The WIB Hamiltonian is $\hat{\mathcal{H}}^{\mathrm{WIB}} = \hat{\mathcal{H}}^{\mathrm{WIB}}_{\mathrm{linear}} + \hat{\mathcal{H}}^{\mathrm{WIB}}_{\mathrm{nonlinear}}$ with

$$\hat{\mathcal{H}}^{\mathrm{WIB}}_{\mathrm{linear}} = \sum_{k\sigma} \omega_k \hat{a}^{\dagger}_{k\sigma}\hat{a}_{k\sigma} + \sum_{k\sigma} \Omega_k \hat{B}^{\dagger}_{k\sigma}\hat{B}_{k\sigma} + g\sum_{k\sigma}\left(\hat{B}^{\dagger}_{k\sigma}\hat{a}_{k\sigma} + \mathrm{h.c.}\right), \tag{25}$$

$$\begin{aligned}\hat{\mathcal{H}}^{\mathrm{WIB}}_{\mathrm{nonlinear}} = {} & W\sum_{kk'}\sum_{q\neq 0}\hat{B}^{\dagger}_{k+q,+1}\hat{B}^{\dagger}_{k'-q,-1}\hat{B}_{k',-1}\hat{B}_{k,+1} + R\sum_{kk'\sigma}\sum_{q\neq 0}\hat{B}^{\dagger}_{k+q,\sigma}\hat{B}^{\dagger}_{k'-q,\sigma}\hat{B}_{k'\sigma}\hat{B}_{k\sigma} \\ & - G\sum_{kk'\sigma}\sum_{q\neq 0}\left(\hat{B}^{\dagger}_{k+q,\sigma}\hat{B}^{\dagger}_{k'-q,\sigma}\hat{B}_{k'\sigma}\hat{a}_{k\sigma} + \mathrm{h.c.}\right),\end{aligned} \tag{26}$$

where $\hat{a}^{\dagger}_{k\sigma}$ and $\hat{a}_{k\sigma}$ are the operators of a photon of momentum $\boldsymbol{k}$ and angular momentum (circular polarization) $\sigma = \pm 1$, and ω_k (Ω_k) is the energy dispersion of a photon (a boson). Kuwata-Gonokami *et al* calculated the matrix-elements of the cavity-polariton scatterings and found that this simple phenomenology can reproduce all the experimental results, in particular, the polarization dependence. Ratios among W, R and G can be determined by comparing with the experiments. This shows that the bosonic treatments are thought to be an effective tool for the description of excitonic nonlinearities.

We here note that the 1s Wannier exciton is not a pure-boson but a quasiboson. Its creation operator is defined through $\hat{b}^{\dagger}_{\boldsymbol{K}\mu\nu} \equiv \sum_{\boldsymbol{k}} f^{(2)}(\boldsymbol{k})\,\hat{c}^{\dagger}_{\alpha\boldsymbol{K}+\boldsymbol{k},\mu}\hat{d}^{\dagger}_{\beta\boldsymbol{K}-\boldsymbol{k},\nu}$, where μ (ν) is a quantum number of the total angular momentum of an electron (a hole), $\alpha = m^*_{\mathrm{e}}/(m^*_{\mathrm{e}} + m^*_{\mathrm{h}})$, $\beta = m^*_{\mathrm{h}}/(m^*_{\mathrm{e}} + m^*_{\mathrm{h}})$, and $f^{(2)}(\boldsymbol{k}) = (\sqrt{2\pi}/L)\left(1 + k^2/4\right)^{-3/2}$ describes the Fourier transform of the electron–hole relative wavefunction in $d = 2$. This exciton operator satisfies the commutation relation:

$$[\hat{b}_{\boldsymbol{K}_1\mu_1\nu_1}, \hat{b}^{\dagger}_{\boldsymbol{K}_2\mu_2\nu_2}] = \delta_{\boldsymbol{K}_1\boldsymbol{K}_2}\delta_{\mu_1\mu_2}\delta_{\nu_1\nu_2} - \hat{\xi}(\boldsymbol{K}_1\mu_1\nu_1|\boldsymbol{K}_2\mu_2\nu_2), \tag{27}$$

where

$$\begin{aligned}\hat{\xi}(\boldsymbol{K}_1\mu_1\nu_1|\boldsymbol{K}_2\mu_2\nu_2) = {} & \delta_{\nu_1\nu_2}\sum_{\boldsymbol{k}} f^{(2)}(\boldsymbol{k})\,f^{(2)}(\alpha\boldsymbol{K}_2 - \alpha\boldsymbol{K}_1 + \boldsymbol{k})\,\hat{c}^{\dagger}_{\beta\boldsymbol{K}_2-\beta\boldsymbol{K}_1+\alpha\boldsymbol{K}_2+\boldsymbol{k},\mu_2}\hat{c}_{\alpha\boldsymbol{K}_1+\boldsymbol{k},\mu_1} \\ & + \delta_{\mu_1\mu_2}\sum_{\boldsymbol{k}} f^{(2)}(\boldsymbol{k})\,f^{(2)}(\alpha\boldsymbol{K}_1 - \alpha\boldsymbol{K}_2 + \boldsymbol{k})\,\hat{d}^{\dagger}_{\alpha\boldsymbol{K}_2-\alpha\boldsymbol{K}_1+\beta\boldsymbol{K}_1-\boldsymbol{k},\nu_2}\hat{d}_{\beta\boldsymbol{K}_1-\boldsymbol{k},\nu_1}.\end{aligned} \tag{28}$$

The second term $\hat{\xi}$ of the right-hand side describes the deviation from the pure-boson commutation relation. Note here that two single-exciton states are orthogonal: $\langle 0|\hat{b}_{\boldsymbol{K}_1\mu_1\nu_1}\hat{b}^{\dagger}_{\boldsymbol{K}_2\mu_2\nu_2}|0\rangle = \delta_{\boldsymbol{K}_1\boldsymbol{K}_2}\delta_{\mu_1\mu_2}\delta_{\nu_1\nu_2}$, while that of two two-exciton states is no longer orthogonal:

$$\begin{aligned}&\langle 0|\hat{b}_{\boldsymbol{K}_4\mu_4\nu_4}\hat{b}_{\boldsymbol{K}_3\mu_3\nu_3}\hat{b}^{\dagger}_{\boldsymbol{K}_1\mu_1\nu_1}\hat{b}^{\dagger}_{\boldsymbol{K}_2\mu_2\nu_2}|0\rangle \\ &\quad = \delta_{\boldsymbol{K}_1\boldsymbol{K}_3}\delta_{\mu_1\mu_3}\delta_{\nu_1\nu_3}\delta_{\boldsymbol{K}_2\boldsymbol{K}_4}\delta_{\mu_2\mu_4}\delta_{\nu_2\nu_4} + \delta_{\boldsymbol{K}_1\boldsymbol{K}_4}\delta_{\mu_1\mu_4}\delta_{\nu_1\nu_4}\delta_{\boldsymbol{K}_2\boldsymbol{K}_3}\delta_{\mu_2\mu_3}\delta_{\nu_2\nu_3} \\ &\qquad - \delta_{\boldsymbol{K}_1+\boldsymbol{K}_2,\boldsymbol{K}_3+\boldsymbol{K}_4}\left(\delta_{\mu_1\mu_3}\delta_{\nu_1\nu_4}\delta_{\mu_2\mu_4}\delta_{\nu_2\nu_3} + \delta_{\mu_1\mu_4}\delta_{\nu_1\nu_3}\delta_{\mu_2\mu_3}\delta_{\nu_2\nu_4}\right) \\ &\qquad \times F(\alpha(\boldsymbol{K}_1 - \boldsymbol{K}_3), \beta(\boldsymbol{K}_2 - \boldsymbol{K}_3)),\end{aligned} \tag{29}$$

where $|0\rangle$ is the ground state and $F(\boldsymbol{K}, \boldsymbol{K}') \equiv \sum_{\boldsymbol{k}} f^{(2)}(\boldsymbol{K} + \boldsymbol{k})\,f^{(2)}(\boldsymbol{K}' + \boldsymbol{k})\,f^{(2)}(\boldsymbol{k})\,f^{(2)}(\boldsymbol{K} + \boldsymbol{K}' + \boldsymbol{k})$. The quasi-boson nature and the nonorthogonality of two two-exciton states are key points for formulating new boson-picture theories of few-exciton systems.

Before the above phenomenological WIB model, there were many theoretical trials to describe many-exciton systems in terms of bosons in the study of the exciton Bose–Einstein condensation [37, 38]. Recently, theoreticians have been interested in how to bosonize a few exciton systems with the spin degrees of freedom, how to evaluate interactions among the bosons and photons [39], and how to cope with the deviation of the pure-boson commutation relations. Inoue *et al* approximated the 1s Wannier exciton in $d = 2$ as a pure-boson to derive the attractive (W) and repulsive (R) interactions between the bosons depending on the total angular momentum [40]. This means that the phenomenological cavity-polariton model gets its basis from a microscopic viewpoint. Recently, Takayama *et al* investigated numerically a scattering problem of two excitons [41], and Combescot *et al* proposed a new treatment of the exciton bosonization [42]. We note here that the validity and limitations of the boson-picture treatment should always be recognized; for example, the decay processes and the detuning effects are hard to be incorporated there.

There are several schemes for bosonization: the Usui transformation [43] for quasibosons [44], the Marumori-mapping technique [45], and an exact mapping to a pure-boson space [46, 47]. Based on these works, Okumura and Ogawa derived a bosonized Hamiltonian describing two-exciton correlation of semiconductor-photon coupled systems with a new bosonization method, which takes into full account an effect of deviation of the excitons from ideal bosons [48]. This deviation effect stems from the fact that the excitons are composite particles, whose character appears clearly in the case where the excitons overlap with each other. They call this effect a 'composite-particle effect' (CPE). The derived bosonized Hamiltonian describes boson–boson interaction and boson–photon nonlinear coupling, and includes the results of the previous works as low-order terms of the CPE. They showed that the CPE brings about enhancement of exciton–exciton scattering strength and qualitative change of photo-transition amplitude. It is also shown that the Hamiltonian describes two-exciton bound and scattering states, both of which play important roles in the four-wave-mixing processes [49]. Moreover, they clarified how deformation of a 1s type exciton wavefunction affects the four-wave-mixing signals near 1s-exciton resonance in a quantum well [49].

Here we make a comment on the bosonization. In the 'exciton bosonization', two fermions in different bands, an electron in a conduction band and a hole in a valence band across the energy gap, are simultaneously mapped to a boson. In the low-density limit of excitons, the bosonic excitons satisfy the pure-boson commutation relation, while boson approximation becomes worse in the high-density limit, as shown in equation (27). On the other hand, as will be shown in the following sections, another bosonization is frequently used to describe low-energy excitations near the Fermi level in degenerate electron systems [50, 51]. A pair of a particle and a vacancy across the Fermi level is treated as a long-wavelength boson, i.e. two fermions in the same band are mapped to a boson. In other words, the charge and spin density fluctuations of an electron gas (or a hole gas) are quantized to be bosons. In particular, the low-energy bosons near the Fermi level in $d = 1$ satisfy the pure-boson commutation relation, thus they are called the Tomonaga bosons [52, 53]. With the use of this property, one of the exactly solvable quantum models, the Tomonaga–Luttinger (TL) model, has been proposed, in which interacting fermions can be described as independent bosons [52].

6. Quantum orders in one-dimensional electron–hole systems

We consider a high-density electron–hole system in $d = 1$ under irradiation by an intense light pulse. What will happen as the number of excitons are increased in semiconductors is a long-standing problem in which both the quantum many-body effects and the nonequilibrium characters should be considered [54, 55]. Since the mean-field approximation is invalid in low

dimensions as mentioned earlier, here we shall make use of the exactly solvable models to avoid ambiguities due to some approximations.

With irradiation of an intense laser pulse to undoped semiconducting wires, we can explore the many-body effects in a $d = 1$ high-density electron–hole system, whose quasiequilibrium states are treated as a two-band TL liquid. Densities of electrons (in the conduction band) and holes (in the valence band) are assumed to be equal to each other, both of which are high enough so that the Fermi points are well-defined in both bands. We further assume that this system is in quasiequilibrium within a radiative lifetime (rigid Fermi-sea picture) [56]. Here we concentrate on the $d = 1$ high-density electron–hole system with the same Fermi wavevector $k_{\rm F}$ for both the conduction and valence bands.

In this system, low-energy excitations near each quasi-Fermi level are important for quantum orderings and their dynamical responses. Then the bosonization method is used to treat the collective excitations of the degenerate electrons and holes. To this end, we linearize the dispersions near the Fermi points with the Fermi velocities of the conduction and valence bands, $v_{\rm F}^{\rm e} \propto (m_{\rm e}^*)^{-1}$ and $v_{\rm F}^{\rm h} \propto (m_{\rm h}^*)^{-1}$. Each band consists of two branches corresponding to the right-moving ($j = 1$) and the left-moving ($j = 2$) particles. The interparticle interaction matrix element is assumed to be spin-independent and parameterized to the nine interaction matrix elements: $g_i^{\rm e}$, $g_i^{\rm h}$ and $g_i^{\rm eh}$ for $i = 1, 2, 4$. We study here the forward-scattering model, which includes essentially only intrabranch interactions, g_2 ($g_2^{\rm e}$, $g_2^{\rm h}$ and $g_2^{\rm eh}$) and is solved exactly.

One advantage of the bosonization method comes from the fact that electron (or hole) field operators can be written in terms of the phase fields, or equivalently, boson creation and annihilation operators, e.g.,

$$\hat{\psi}_{1\sigma}^{\rm e}(x) = (2\pi\alpha)^{-1/2}{\rm e}^{{\rm i}k_{\rm F}x}\exp\left[\frac{\rm i}{2}\{\hat{\theta}_{\rm e}(x) + \hat{\theta}_{\rm e}^{-}(x) + \sigma[\hat{\phi}_{\rm e}(x) + \hat{\phi}_{\rm e}^{-}(x)]\} + {\rm i}\hat{\varphi}_{1\sigma}^{\rm e}\right], \tag{30}$$

$$\hat{\psi}_{2\sigma}^{\rm e}(x) = (2\pi\alpha)^{-1/2}{\rm e}^{-{\rm i}k_{\rm F}x}\exp\left[-\frac{\rm i}{2}\{\hat{\theta}_{\rm e}(x) - \hat{\theta}_{\rm e}^{-}(x) + \sigma[\hat{\phi}_{\rm e}(x) - \hat{\phi}_{\rm e}^{-}(x)]\} + {\rm i}\hat{\varphi}_{2\sigma}^{\rm e}\right], \tag{31}$$

for the electron fields of branches $j = 1$ and 2, respectively, where α is a cutoff and $\hat{\varphi}_{j\sigma}^{\rm e}$ is necessary for ensuring the anticommutation relation of $\hat{\psi}_{j\sigma}^{\rm e}$ with different j and σ. Using the phase variables, we obtain a phase Hamiltonian of the two-band TL liquid: $\hat{\mathcal{H}} \equiv \hat{\mathcal{H}}^{\rm charge} + \hat{\mathcal{H}}^{\rm spin}$, where

$$\hat{\mathcal{H}}^{\rm charge} = \int {\rm d}x\,\{A_{\rm e}\hat{P}_{\rm e}^2(x) + C_{\rm e}[\nabla\hat{\theta}_{\rm e}(x)]^2 + A_{\rm h}\hat{P}_{\rm h}^2(x) + C_{\rm h}[\nabla\hat{\theta}_{\rm h}(x)]^2 + 2C_{\rm eh}\nabla\hat{\theta}_{\rm e}(x)\nabla\hat{\theta}_{\rm h}(x)\}, \tag{32}$$

$$\hat{\mathcal{H}}^{\rm spin} = \int {\rm d}x\,\{B_{\rm e}\hat{\Pi}_{\rm e}^2(x) + D_{\rm e}[\nabla\hat{\phi}_{\rm e}(x)]^2 + B_{\rm h}\hat{\Pi}_{\rm h}^2(x) + D_{\rm h}[\nabla\hat{\phi}_{\rm h}(x)]^2\}. \tag{33}$$

Here $\hat{\theta}_{\rm e}(x)$ [$\hat{\theta}_{\rm h}(x)$] is the charge phase of the conduction [valence] electrons, whose conjugate momentum is $\hat{P}_{\rm e}(x) \equiv -(4\pi)^{-1}\partial\hat{\theta}_{\rm e}^{-}(x)/\partial x$ [$\hat{P}_{\rm h}(x) \equiv -(4\pi)^{-1}\partial\hat{\theta}_{\rm h}^{-}(x)/\partial x$], while $\hat{\phi}_{\rm e}(x)$ [$\hat{\phi}_{\rm h}(x)$] is the spin phase, whose conjugate momentum is $\hat{\Pi}_{\rm e}(x) \equiv -(4\pi)^{-1}\partial\hat{\phi}_{\rm e}^{-}(x)/\partial x$ [$\hat{\Pi}_{\rm h}(x) \equiv -(4\pi)^{-1}\partial\hat{\phi}_{\rm h}^{-}(x)/\partial x$]. Coefficients are given by $A_\nu \equiv 2\pi(\bar{v}_{\rm F}^\nu - g_2^\nu)$, $B_\nu \equiv 2\pi\bar{v}_{\rm F}^\nu$, $C_\nu \equiv (\bar{v}_{\rm F}^\nu + g_2^\nu)/8\pi$, $D_\nu \equiv \bar{v}_{\rm F}^\nu/8\pi$ and $C_{\rm eh} \equiv g_2^{\rm eh}/4\pi$, where $\nu = e$ or h and $\bar{v}_{\rm F}^\nu \equiv v_{\rm F}^\nu + g_4^\nu$ is the normalized Fermi velocity. The charge part of the forward-scattering Hamiltonian, $\hat{\mathcal{H}}^{\rm charge}$, is diagonalized by the unitary transformation: $(\hat{\theta}_{\rm e}, \hat{\theta}_{\rm h}) \to (\hat{\theta}_1, \hat{\theta}_2)$ via

$$\begin{bmatrix}\hat{\theta}_{\rm e}\\ \hat{\theta}_{\rm h}\end{bmatrix} = \begin{bmatrix}\sqrt{A_{\rm e}}\cos\Theta & -\sqrt{A_{\rm e}}\sin\Theta\\ \sqrt{A_{\rm h}}\sin\Theta & \sqrt{A_{\rm h}}\cos\Theta\end{bmatrix}\begin{bmatrix}\hat{\theta}_1\\ \hat{\theta}_2\end{bmatrix}, \tag{34}$$

with Θ being given by $\tan 2\Theta \equiv 2C_{\rm eh}\sqrt{A_{\rm e}A_{\rm h}}/(A_{\rm e}C_{\rm e} - A_{\rm h}C_{\rm h})$. Consequently, the diagonalized forward-scattering Hamiltonian becomes $\hat{\mathcal{H}}_{\rm forward} = \int {\rm d}x \sum_{i=1,2}\{\hat{P}_{\rm i}^2(x) + [v_{\rm charge}^{(i)}\nabla\hat{\theta}_{\rm i}(x)]^2\} + \hat{\mathcal{H}}^{\rm spin}$, where $\hat{P}_{\rm i}$ is the conjugate momentum for $\hat{\theta}_{\rm i}$ ($\hat{\mathcal{H}}^{\rm spin}$ is already diagonalized). We find that the motions of four phases, $\hat{\theta}_1$, $\hat{\theta}_2$, $\hat{\phi}_{\rm e}$ and $\hat{\phi}_{\rm h}$, are described by massless acoustic modes, which have linear dispersions in their excitation spectra. The velocities of the transformed charge phases, $\hat{\theta}_1$ and $\hat{\theta}_2$, are given by

$$v_{\rm charge}^{(i)} = \left\{2(A_{\rm e}C_{\rm e} + A_{\rm h}C_{\rm h}) \pm 2[(A_{\rm e}C_{\rm e} - A_{\rm h}C_{\rm h})^2 + 4C_{\rm eh}^2 A_{\rm e}A_{\rm h}]^{1/2}\right\}^{1/2}, \qquad (35)$$

respectively, where $i = 1$ (2) corresponds to the + (−) sign of the right-hand side. On the other hand, velocities of the spin phases, $\hat{\phi}_{\rm e}$ and $\hat{\phi}_{\rm h}$, are $v_{\rm F}^{\rm e}$ and $v_{\rm F}^{\rm h}$, respectively: $v_{\rm spin}^{\nu} = v_{\rm F}^{\nu}$.

In $d = 1$ quantum many-particle systems, the competition among various Fermi-surface instabilities occurs through quantum fluctuations even at zero temperature. There are sixteen possible order parameters, $\hat{\mathcal{O}}(x)$. All the correlation functions, $\langle\hat{\mathcal{O}}(x,\tau)\,\hat{\mathcal{O}}^{\dagger}(0,0)\rangle$, behave like $[\max(x,\tau)]^{-\eta}$ for large x and large imaginary time τ. The exponent η for each order parameter is given in [57]. The phase diagram of the quasi-thermal-equilibrium state was given, which is divided into following four regions.

(a) *Exciton Bose–Einstein-condensate phase.* When the repulsive interaction between conduction electrons and valence ones is strong (positive and large $g_2^{\rm eh}$), i.e. the strong attraction between electrons and holes, the exciton Bose–Einstein condensate (exciton BEC) at $K = 0$ predominates. Spin-singlet and triplet exciton Bose condensation are degenerate in our spin-independent forward-scattering model. The exciton density wave at $K = \pm 2k_{\rm F}$ cannot prevail in the whole plane.

(b) *Density-wave phase.* When the repulsion between the electrons within each band is strong (positive and large $g_2^{\rm e}$ or $g_2^{\rm h}$), the charge-density wave (CDW) and the spin-density wave (SDW) predominate. The valence-band electrons (i.e. holes) with heavier mass have the stronger tendency toward ordering. When the velocity ratio $|v_{\rm F}^{\rm h}/v_{\rm F}^{\rm e}|$ is decreased from unity, the CDW and SDW region extends and invades the exciton BEC region.

(c) *Ordinary superconductivity phase.* The attractive interactions, i.e. negative g_2, yield conventional superconductivity (SC). The negative $g_2^{\rm h}$ results in intraband pairing with zero total momentum $K = 0$. The valence-band electrons with heavier mass have the stronger tendency toward ordering.

(d) *Unconventional superconductivity phase.* On the other hand, the negative $g_2^{\rm eh}$ causes *interband* Cooper pairing at $K = \pm 2k_{\rm F}$. This unconventional superconductivity is a peculiar feature of the $d = 1$ system. Singlet and triplet SCs are degenerate in both the above cases.

Recently, we have extended the above model to take into account the long-range Coulomb interaction. The long-range Coulomb interaction enhances the quantum correlation of biexciton formation. That is, the biexciton solid (crystal) or liquid is the most favourable order at zero temperature in $d = 1$. Effects of the electron–hole backward scattering are also re-examined with the self-consistent harmonic approximation and the renormalization-group method. We found that the biexciton solid (crystal) is formed when the electron–hole backward scattering coexists with the forward scattering. Thus, in realistic one-dimensional electron–hole systems, biexciton solid and liquid orders are of particular importance, resulting in the absence of the exciton Mott transition in $d = 1$. Details will be reported elsewhere [58].

We shall discuss the optical absorption spectrum of the degenerate electron–hole system in $d = 1$ [59]. The absorption spectrum, $W_{\rm OPA}(\omega)$, is related to the Fourier transform of the correlation function, $\langle\hat{P}(t)\hat{P}^{\dagger}(0)\rangle$, where the polarization $\hat{P}$ (namely the

dipole operator) is given by $\hat{P}(t) = |M| \int \mathrm{d}x \sum_\sigma \hat{\psi}^{\mathrm{e}\dagger}_\sigma(x,t)\hat{\psi}^{\mathrm{h}}_\sigma(x,t)\mathrm{e}^{\mathrm{i}E_0 t} + \mathrm{h.c.}$, where $\hat{\psi}^\nu_\sigma(x,t) = \exp[\mathrm{i}\hat{\mathcal{H}}t]\hat{\psi}^\nu_\sigma(x)\exp[-\mathrm{i}\hat{\mathcal{H}}t]$ is the Heisenberg representation of the field operator ($\hat{\psi}^\nu_\sigma = \hat{\psi}^\nu_{1\sigma} + \hat{\psi}^\nu_{2\sigma}$), M is an interband matrix element (assumed to be constant), and E_0 is the energy of the absorption and emission edge in the single-electron picture. The correlation function of the dipole operator contains the correlation function $C_{\mathrm{SEBC}}(t) \equiv \langle \hat{\mathcal{O}}_{\mathrm{SEBC}}(x,t)\,\hat{\mathcal{O}}^\dagger_{\mathrm{SEBC}}(0,0)\rangle$ of the order parameter describing the spin-singlet exciton BEC, $\hat{\mathcal{O}}_{\mathrm{SEBC}}(x) \equiv \sum_{j=1,2}\sum_\sigma \hat{\psi}^{\mathrm{e}\dagger}_{j\sigma}(x)\hat{\psi}^{\mathrm{h}}_{j\sigma}(x)$. For large t, the correlation function behaves like $C_{\mathrm{SEBC}}(t) \sim t^{-\eta_{\mathrm{SEBC}}}$. This means that the optical spectrum shows the power-law singularity like $W_{\mathrm{OPA}}(\omega) \sim (\hbar\omega - E_{\mathrm{F}})^\beta \Theta(\hbar\omega - E_{\mathrm{F}})$ in the vicinity of E_{F}, where E_{F} is the absorption-edge energy and β is the critical exponent: $\beta = \eta_{\mathrm{SEBC}} - 2 = \beta^{\mathrm{ex}} + \beta^{\mathrm{c-oc}} + \beta^{\mathrm{v-oc}}$, where

$$\beta^{\mathrm{ex}} = -\frac{\pi[v^{(1)}_{\mathrm{charge}} - v^{(2)}_{\mathrm{charge}}]}{2\sqrt{A_{\mathrm{e}}A_{\mathrm{h}}}}\left[1 + \frac{A_{\mathrm{e}}A_{\mathrm{h}}}{4\pi^2 v^{(1)}_{\mathrm{charge}}v^{(2)}_{\mathrm{charge}}}\right]\sin 2\Theta, \tag{36}$$

$$\beta^{\mathrm{c-oc}} = \frac{A_{\mathrm{h}}s_1}{8\pi v^{(1)}_{\mathrm{charge}}v^{(2)}_{\mathrm{charge}}} + \frac{\pi s_2}{2A_{\mathrm{h}}} - \frac{1}{2}, \tag{37}$$

$$\beta^{\mathrm{v-oc}} = \frac{A_{\mathrm{e}}s_2}{8\pi v^{(1)}_{\mathrm{charge}}v^{(2)}_{\mathrm{charge}}} + \frac{\pi s_1}{2A_{\mathrm{e}}} - \frac{1}{2}. \tag{38}$$

Here $s_{\mathrm{i}} \equiv \frac{1}{2}[v^{(1)}_{\mathrm{charge}} + v^{(2)}_{\mathrm{charge}} \pm (v^{(1)}_{\mathrm{charge}} - v^{(2)}_{\mathrm{charge}})\cos 2\Theta]$ with $i = 1$ (2) corresponding to the + (−) sign. This power-law anomaly in optical spectra near an edge energy is one of the FESs.

We stress that the FES exponent, β, is determined by the correlation exponent, η_{SEBC}, of the order parameter describing the singlet-exciton BEC. Roughly speaking, the divergent edge spectrum (corresponding to $\beta < 0$) can be observed when the electron–hole interaction is attractive ($g^{\mathrm{eh}}_2 > 0$ and $g^{\mathrm{eh}}_4 > 0$), and rather weak electron–electron and hole–hole correlations occur. When the excitons lie completely at the condensation state at zero temperature, an optical spectrum is expected to show a δ-function-like peak if we can ignore the quantum fluctuations. Actually, however, quantum fluctuation can never be neglected in $d = 1$ systems and it tends to destroy the exciton condensation. Consequently, the δ-function-like peak spectrum vanishes and is replaced by the power-law peak, which is really the FES and is a remnant of the exciton BEC. In this sense, the FES results from a fluctuating condensed state of many $d = 1$ excitons. Effects of the randomness were discussed in [57, 59].

7. Gas–liquid phase separation in finite-lifetime systems

Phase separation is the cooperative, nonequilibrium phenomenon that systems of interacting particles change macroscopically. It can also occur in systems of the excited state at finite temperature, for example, in the electron–hole system as the formation of the electron–hole droplet (liquid) in an electron–hole plasma (gas). A characteristic feature of this electron–hole system is that the constituent particles (electrons and holes) have finite lifetime. Recently, dynamics of this phase separation or the spinodal decomposition has been observed experimentally in photoexcited semiconductors [60, 61]. So we will study the phase separation *dynamics* in systems of unstable particles created by the external field assuming the particles are classical. Sugakov and the present author extended the Langer, Bar-on and Miller (LBM) theory into finite lifetime systems, in which particles have creation and annihilation processes [62–64]. Based on this extension, we formulated the theory based on the coarse-grained lattice gas model and take into account the creation and annihilation processes of particles [65].

In a study of the phase separation, the particle density is often used as the order parameters. So, in our theory, the space is divided into many cells. We assumed that particles are distributed

in one cell and that there is an upper limit N of the intracell particle number. After this coarse-graining procedure with cells, the coarse-grained Hamiltonian was introduced;

$$H = -\tfrac{1}{2}\sum_i \sum_{j(\neq i)} J_{|i-j|} n_i n_j - K \sum_i n_i^2. \tag{39}$$

The interparticle interaction is divided into two parts. One is the long-range intercell interaction $J_{|i-j|}$ between two different cells. Another is the short-range intracell interaction K within only one cell. The order parameter is the intracell particle number n_i, which is continuous, $0 \leqslant n_i \leqslant N$. Moreover we introduce two parameters for the intercell interaction $J_{|i-j|}$; the strength $J_0 \equiv \sum_{j(\neq i)} J_{|i-j|}$ and the range $R \equiv \frac{1}{\sqrt{J_0}}[\sum_{j(\neq i)} (\boldsymbol{r}_j - \boldsymbol{r}_i)^2 J_{|i-j|}]^{1/2}$.

The temporal development of a system is described by two physical quantities. One is the single-point distribution function; $P^{(1)}(n_\alpha, t) \equiv \int \prod_{i(\neq\alpha)} \mathrm{d}n_i P(n_1, \ldots, n_\alpha, \ldots, n_N, t)$. This can be interpreted as the distribution function of the intracell particle number. Another is the dynamical structure factor; $S(\boldsymbol{k}, t) \equiv \sum_\alpha \exp[-\mathrm{i}\boldsymbol{k} \cdot (\boldsymbol{r}_\alpha - \boldsymbol{r}_\beta)][\langle n_\alpha n_\beta \rangle - \langle n^2 \rangle(t)]$. This is concerned directly with the spectrum of the light scattering. With the use of Binder's master equation method and the LBM approximation, we derived the closed-form coupled equation describing the temporal development of $P^{(1)}(n, t)$ and $S(\boldsymbol{k}, t)$. Processes of the particle creation and annihilation were taken into account as the competition between the creation due to the external creation rate $y(t)$ and the decay due to the finite lifetime τ.

We investigated analytically effects of the finite lifetime for the phase separation dynamics in the early stages with the linear approximation. We define the fluctuation modes of the intracell particle number as $n_{\boldsymbol{k}}(t) \equiv \langle n \rangle \delta(\boldsymbol{k}) + C \exp[\Gamma_k t]$. The second term is the fluctuation from the uniform density state. Γ_k is called the Lyapunov spectrum. If $\Gamma_k > 0$, the fluctuation modes with the wavenumber k can grow, but if $\Gamma_k < 0$, the fluctuation modes decay. In the linear approximation, it can be evaluated as

$$\Gamma_k \propto -Ak^2 \left[k^2 + \frac{2}{R^2 T_\mathrm{C}} (T - T_\mathrm{C}) \right] - \frac{1}{\tau} \tag{40}$$

with a positive constant A and the critical temperature $T_\mathrm{C} \equiv \frac{N}{4}(J_0 + 2k)$. Thus, the finite lifetime ($\tau < \infty$) makes Γ_k smaller. We consider the steady creation case when the creation rate is set by $y(t) = \langle n \rangle / \tau = \text{constant}$, so that the mean intracell particle number becomes constant $\langle n \rangle$ by the competition with the finite lifetime τ. The system is isotropic and translational symmetric, so the wavenumber $\boldsymbol{k}$ can be replaced by its amplitude $k \equiv |\boldsymbol{k}|$. We can define the critical wavenumber as the boundary wavenumber between increase [$\Gamma_k > 0$] and decrease [$\Gamma_k < 0$] of the fluctuation modes. In the case with creation [$y(t) = \text{constant}$] and annihilation [$\tau = \text{finite}$], *two* critical wavenumbers can be defined; the lower critical wavenumber $k_\mathrm{C}^{(1)}$ and the upper critical wavenumber $k_\mathrm{C}^{(2)}$. Due to the effect of the finite lifetime, the lower critical wavenumber $k_\mathrm{C}^{(1)}$ newly appears and the growth of the fluctuation modes with the wavelength $k^{-1} > [k_\mathrm{C}^{(1)}]^{-1}$ is restrained.

Numerical results are explained here. We consider the steady creation case when $\langle n \rangle = \text{constant}$ and $y(t) = \langle n \rangle / \tau = \text{constant}$. In the initial state, the particle density is distributed uniformly. So $P^{(1)}(n, t = 0)$ is Gaussian with the variance 0.002 25, in which the thermal fluctuation is also considered, and $S(k, t = 0) = 0$. The quantities are normalized by the following units; N for the particle number, the inverse of the cell size a_0^{-1} for wavenumber, the shortest time of the particle transfer between neighbouring cells τ_0 for time, the critical temperature T_C for temperature, $k_\mathrm{B} T_\mathrm{C}/N$ for the interaction coefficients.

Figure 1 shows the temporal developments of $P^{(1)}(n, t)$ and $S(k, t)$. Figures 1(a) and (b) show the behaviours in the case of $y(t) = 0$ and $\tau = \infty$. From figure 1(a) we find that $P^{(1)}(n, t)$ separates into two peaks completely. This indicates that the phase separation can

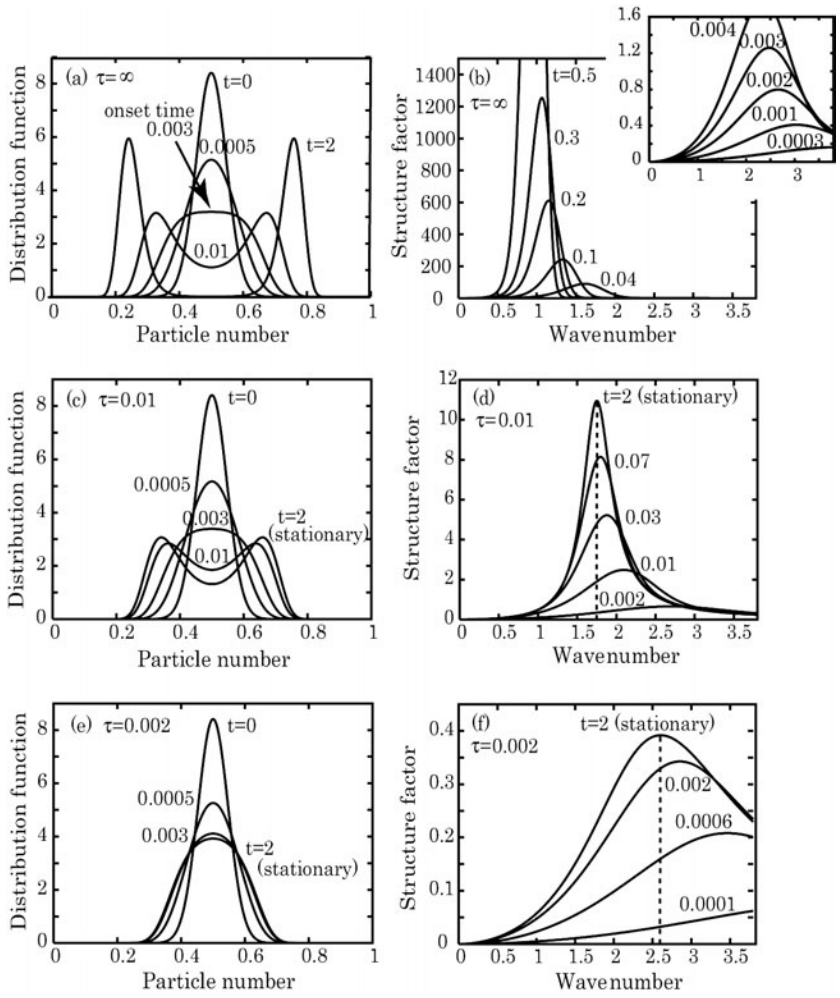

Figure 1. Temporal development of the single-point distribution function $P^{(1)}(n,t)$ and the dynamical structure factor $S(k,t)$ for $J_0R^2 = 0.08$, $T = 0.88$, $N = 1000$, $v_0 = 0.01$ and $n_0 = 0.5$. The creation rate is $y = n_0/\tau = 0.5/\tau$. The three figures in the left row, (a), (c) and (e), are $P^{(1)}(u,t)$ and ones in the right row, (b), (d) and (f), are $S(k,t)$. The lifetime of particles is $\tau = \infty$ for (a) and (b), 0.01 for (c) and (d), and 0.002 for (e) and (f). The inset of (b) shows the behaviour during $0 \leqslant t \lesssim 0.004$. In (c)–(f) for the case of the finite lifetime, the states with '$t = 2$ (stationary)' can be considered as stationary ones. Units are defined as the following: N for particle number and a_0^{-1} for wavenumber.

occur. The onset time t_{onset} can be defined as a time when $P^{(1)}(n,t)$ begins separating and this is when the order formation begins. We also investigated the temperature-dependence of the onset time. When temperature approaches the critical temperature, the onset time increases rapidly. This may be the manifestation of the critical slowing down. From figure 1(b), we find that the dynamical structure factor grows and that the characteristic wavenumber $k_{\max}(t)$, at which $S(k,t)$ has a maximum peak, eventually becomes $k_{\max}(t \to \infty) \to 0$. This manifests that the system separates completely into two phases in the final state.

Figures 1(c)–(f) show the behaviour in the case of $\tau =$ finite and $y(t) = \langle n \rangle/\tau =$ constant. From figures 1(c) and (e), we find that the order formation can occur in the case of

$\tau = 0.01 > t_{\rm onset}$, but it cannot occur in the case of $\tau = 0.002 < t_{\rm onset}$. Figures 1(d) and (f) show that the increase of $S(k,t)$ stops. From figure 1(f), in particular, we find that the thermal-fluctuation part proportional to k^2 is dominant when the lifetime is short enough. The characteristic wavenumber $k_{\rm max}(t)$ also approaches the finite value at $t \to \infty$. This manifests that the finite size $[k_{\rm max}(t \to \infty)]^{-1}$ eventually remains. We found the power-law dependence of $[k_{\rm max}(t \to \infty)]^{-1}$ on τ and J_0R^2: $[k_{\rm max}(t \to \infty)]^{-1} \propto \tau^{1/4}$ and $[k_{\rm max}(t \to \infty)]^{-1} \propto (J_0R^2)^{1/4}$. In order to extend our theory to exciton and electron–hole systems, the quantum nature of the particles is important. This work is in progress [66].

8. Fermi-surface effects in optical transitions of one-dimensional metals

Here we consider an exciton (the Mahan exciton) in low-dimensional degenerate (doped) semiconductors or in low-dimensional metals. Several optical transition probabilities reflect the final-state interaction due to an optically generated hole potential. This interaction brings about two kinds of intrinsic dynamical effects in degenerate electron systems: an orthogonality catastrophe and a many-body excitonic correlation [67]. The former suppresses the transition but the latter enhances it. This is a characteristic point in contrast to those in semiconductors. We shall discuss these effects in $d = 1$. The most striking feature in optical responses of the TL liquids is the power-law singularity, which is characterized by some critical exponents. We pay attention to the valence-band photoemission spectrum, the core-level photoemission spectrum and the OPA spectrum. These optical transition processes yield the power-law anomaly in the edge spectra with different critical exponents [68, 69].

The $d = 1$ degenerate electron systems near the Fermi level are characterized by two (right- and left-moving) branches of electrons. When the interparticle interaction in $d = 1$ is of the short-range type, the Coulomb scattering strengths are represented by constant parameters: g_2, g_4 and g_1 with conventional notation [53], where g_2 and g_4 correspond to the strengths of inter- and intra-branch forward scatterings, and g_1, the backward-scattering strength. Then the backward scattering is neglected because $|g_2| \simeq |g_4| \gg |g_1|$. We further classify the interaction parameters in terms of the mutual spin orientation; the scattering between parallel-spin ($\parallel$) particles and that between antiparallel-spin ($\perp$) ones are labelled separately as $g_{i\parallel}$ and $g_{i\perp}$, respectively, for $i = 2, 4$. For convenience, we define the parameters, K_ρ and K_σ, for characterizing the interaction, i.e. $K_\nu \equiv [(v_{\rm F} + g_{4\nu} - g_{2\nu})/(v_{\rm F} + g_{4\nu} + g_{2\nu})]^{1/2}$ for $\nu = \rho$ (charge degree of freedom) or σ (spin) with $g_{i\rho} \equiv (g_{i\parallel} + g_{i\perp})/2$, $g_{i\sigma} \equiv (g_{i\parallel} - g_{i\perp})/2$, and $v_{\rm F}$ is the spin-independent Fermi velocity.

According to the usual bosonization, we linearize the conduction-band dispersion near the Fermi points: $\epsilon(k) \simeq \sum_j \epsilon_j(k)$ with $\epsilon_j(k) \equiv \pm v_{\rm F}(k \mp k_{\rm F})$, where $k_{\rm F}$ is the Fermi wavenumber and $j = 1$ ($j = 2$) corresponds to the right- (left-) moving branch. In this case, the $d = 1$ electron systems are described by the following Hamiltonian: $\hat{H}^{\rm e} = \hat{H}^{\rm e}_0 + \hat{H}^{\rm e}_{\rm int}$, where

$$\hat{H}^{\rm e}_0 = \frac{2\pi v_{\rm F}}{L} \sum_s \sum_{p>0} \left[\hat{\varrho}_{1{\rm s}}(p)\hat{\varrho}_{1{\rm s}}(-p) + \hat{\varrho}_{2{\rm s}}(-p)\hat{\varrho}_{2{\rm s}}(p) \right], \tag{41}$$

$$\begin{aligned} \hat{H}^{\rm e}_{\rm int} = {} & \frac{\pi}{L} \sum_{s,s'} (g_{2\parallel}\delta_{s,s'} + g_{2\perp}\delta_{s,-s'}) \sum_{p>0} \left[\hat{\varrho}_{1{\rm s}}(p)\hat{\varrho}_{2s'}(-p) + \hat{\varrho}_{1{\rm s}}(-p)\hat{\varrho}_{2s'}(p) \right] \\ & + \frac{\pi}{L} \sum_{s,s'} (g_{4\parallel}\delta_{s,s'} + g_{4\perp}\delta_{s,-s'}) \sum_{p>0} \left[\hat{\varrho}_{1{\rm s}}(p)\hat{\varrho}_{1s'}(-p) + \hat{\varrho}_{2{\rm s}}(-p)\hat{\varrho}_{2s'}(p) \right] \end{aligned} \tag{42}$$

and $\hat{\varrho}_{js}(p) \equiv \sum_k \hat{c}^\dagger_{j,k+p,s}\hat{c}_{jks}$ is the spin-dependent density-fluctuation operator for spin $s = \uparrow, \downarrow = \pm 1$ in the jth branch, which obeys boson commutation relations. The electronic Hamiltonian, $\hat{H}^{\rm e}$, is described also as a sum of two diagonal parts describing the charge- and

spin-density fluctuations: $\hat{\mathcal{H}}^{\rm e} = \sum_{\nu=\rho,\sigma}\sum_{p>0} v_\nu p\,(\hat{\alpha}^\dagger_{\nu p}\hat{\alpha}_{\nu p} + \hat{\beta}^\dagger_{\nu p}\hat{\beta}_{\nu p})$. Here $\hat{\alpha}_{\rho p}$ and $\hat{\beta}_{\rho p}$ ($\hat{\alpha}_{\sigma p}$ and $\hat{\beta}_{\sigma p}$) are boson operators for the charge (spin) fluctuation, which are related to the density-fluctuation operators via $\hat{\alpha}^\dagger_{\nu p} = (\pi/Lp)^{1/2}\sum_{s=\pm1}[\hat{\varrho}_{1s}(p)\cosh\gamma_{\nu p} \pm \hat{\varrho}_{2s}(p)\sinh\gamma_{\nu p}]$ and $\hat{\beta}_{\nu p} = (\pi/Lp)^{1/2}\sum_{s=\pm1}\left[\hat{\varrho}_{2s}(p)\cosh\gamma_{\nu p} \pm \hat{\varrho}_{1s}(p)\sinh\gamma_{\nu p}\right]$ for $\nu = \rho, \sigma$ with $\cosh(2\gamma_{\nu p}) = v_{\rm F}(1+g_{2\nu})/v_\nu$ and $\sinh(2\gamma_{\nu p}) = v_{\rm F}g_{2\nu}/v_\nu$. Both the charge and spin density fluctuations have linear gapless dispersions with constant velocities:

$$v_\nu = \frac{2(v_{\rm F}+g_{4\nu})}{K_\nu + K_\nu^{-1}} = [(v_{\rm F}+g_{4\nu})^2 - g_{2\nu}^2]^{1/2}, \tag{43}$$

for $\nu = \rho, \sigma$.

Peculiar features of the TL liquid are found in its dynamical properties, which are characterized by anomalous power laws in correlation functions. We shall study the single-electron Green function: $G^{\rm e}_{js}(x,t) = -{\rm i}\Theta(t)\langle\hat{\psi}_{js}(x,t)\hat{\psi}^\dagger_{js}(0,0)\rangle$, where $\Theta(t)$ is the unit-step function and $\hat{\psi}_{js}(x,t)$ is the Heisenberg representation of the field operator $\hat{\psi}_{js}(x)$ for an electron in the jth branch with spin s. The average is made by the Fermi vacuum at zero temperature. Using the diagonalized Hamiltonian, we have

$$G^{\rm e}_{js}(x,t) = \frac{{\rm e}^{\pm{\rm i}k_{\rm F}x}}{2\pi}\lim_{\delta\to0}\frac{\Lambda + {\rm i}(v_{\rm F}t \mp x)}{\delta + {\rm i}(v_{\rm F}t \mp x)}\prod_{\nu=\rho,\sigma}\frac{1}{\sqrt{\Lambda + {\rm i}(v_\nu t \mp x)}}\left[\frac{\Lambda^2}{(\Lambda + {\rm i}v_\nu t)^2 + x^2}\right]^{\gamma^\nu_{\rm TL}}, \tag{44}$$

where $j = 1$ (2) corresponds to the upper (lower) sign of the right-hand side, Λ and δ are cutoffs, and the exponent is $\gamma^\nu_{\rm TL} = (1/8)(K_\nu + K_\nu^{-1} - 2) \geqslant 0$. Equation (44) gives a universal behaviour of the Green function, which is independent of detailed cutoff forms. For $t = 0$, the single-electron Green function decays as $G^{\rm e}_{js}(x,0) \sim x^{-\beta_{\rm TL}-1}$ with the exponent $\beta_{\rm TL} \equiv 2\left(\gamma^\rho_{\rm TL} + \gamma^\sigma_{\rm TL}\right) \geqslant 0$, which appears in all single-electron properties; e.g., the momentum distribution function $n(k) \sim 1/2 - C|k-k_{\rm F}|^{\beta_{\rm TL}}\,{\rm sign}(k-k_{\rm F})$ (here C is a positive constant) and the single-particle density of states $N(\omega) \sim |\omega|^{\beta_{\rm TL}}$. The critical exponent $\beta_{\rm TL}$ is rewritten as

$$\beta_{\rm TL} = \frac{1}{4}\left(K_\rho + K_\rho^{-1} + K_\sigma + K_\sigma^{-1}\right) - 1 = \frac{1}{2}\sum_{\nu=\rho,\sigma}\left[1 - \left(\frac{g_{2\nu}}{v_{\rm F}+g_{4\nu}}\right)^2\right]^{-1/2} - 1 \geqslant 0. \tag{45}$$

Before the optical transition occurs, we assume that the partially filled band has N electrons forming the TL liquid and there is no positive hole in any levels and bands. Hereafter this initial state is called the N-electron–0-hole state, denoted as the $(N,0)$ state. In this section, we consider three types of final states after optical transitions.

(a) *From* $(N,0)$ *to* $(N-1,0)$. After an electron in the N-electron TL system is excited to be emitted as a photoelectron, the final state is the $(N-1,0)$ state, where no optical hole is generated and the number of electrons only decreases by one.

(b) *From* $(N,0)$ *to* $(N,1)$. When an electron in a core (valence) level is excited by a larger-energy photon to be detected as a photoelectron, the final state is $(N,1)$, where the number of electrons in the TL liquid remains unchanged and a hole is abruptly generated. Here the Auger processes are neglected.

(c) *From* $(N,0)$ *to* $(N+1,1)$. When an electron in a core level is excited by a photon to an empty state of the partially filled band, the final state is the $(N+1,1)$, where an electron is added to the TL liquid band and a hole is suddenly generated, i.e. the numbers of both electron and hole change simultaneously by one.

8.1. *Valence-band photoemission:* $(N, 0) \to (N-1, 0)$

Valence-band photoemission spectroscopy measures the energy distribution of the photoelectrons ejected from a partially filled band by absorbing photons of a fixed frequency. The valence-band photoemission spectrum $P_{\rm PES}(\epsilon)$ as a function of the photoelectron energy ϵ (measured from the Fermi energy $E_{\rm F}$) reflects directly the density of states $N(\omega)$. Then $P_{\rm PES}(\epsilon) \sim \epsilon^{\beta_{\rm TL}}\Theta(\epsilon)$. The critical exponent $\beta_{\rm TL}$ is given by equation (45). The valence-band photoemission spectrum can be direct evidence for the absence of a discontinuous jump at $k = k_{\rm F}$ in the momentum distribution of the TL liquid. Thus nonzero $\beta_{\rm TL}$ is evidence of the TL liquid.

The valence-band photoemission spectrum is the Fourier transform of the time-domain single-electron Green function $G^{\rm e}_{js}(t) = -{\rm i}\Theta(t)\langle {\rm e}^{{\rm i}t\hat{\mathcal{H}}^{\rm e}/\hbar}\hat{\psi}_{js}{\rm e}^{-{\rm i}t\hat{\mathcal{H}}^{\rm e}/\hbar}\hat{\psi}^{\dagger}_{js}\rangle \sim t^{-\beta_{\rm TL}-1}$, that is, $P_{\rm PES}(\epsilon) \sim (E_{\rm F}-\epsilon)^{\beta_{\rm TL}}$. Thus valence-band photoemission spectroscopy is an effective tool for investigating TL liquid properties, particularly its single-electron properties.

8.2. *Core-level photoemission:* $(N, 0) \to (N, 1)$

Here we mention the orthogonality theorem. When dynamical and local perturbations are applied to degenerate electron systems, low-energy excitations near the Fermi energy come into play and give rise to an infrared divergence [67]. The overlap integral between the total electronic wavefunctions, $|\Psi_{\rm i}\rangle$ and $|\Psi_{\rm f}\rangle$, of the Fermi sea without and with a local potential becomes zero as the system size goes to infinity, i.e. these two states are orthogonal: $|\langle\Psi_{\rm f}|\Psi_{\rm i}\rangle|^2 = n_{\rm F}^{-\beta_{\rm oc}/2}$. Here $n_{\rm F}$ is the number of (s-wave) electrons and $\beta_{\rm oc}$ is the critical exponent for the orthogonality catastrophe. To detect phenomena related to the orthogonality property, the sudden appearance of an external local potential is necessary. This can be done in core-level photoemission spectroscopy.

Core-level photoemission spectroscopy measures the energy distribution of the photoelectrons ejected from a core level in a metal by absorbing photons of a fixed frequency. If the existence of conduction electrons is neglected, only a sharp line will be observed. When the photon energy is high enough for the photoelectron to leave the metal instantly without being affected by a final-state interaction, the sharp line broadens with a long tail on its lower-energy side. For the core-level photoemission spectrum, $P_{\rm core}(\epsilon)$, the probability of finding an ejected electron at an energy ϵ lower than the main peak, is a direct measure of the probability that the conduction electrons will be excited with an excitation energy ϵ due to the hole potential.

When an optical hole with spin $-s$ (an excited electron with spin s) is created, the electron–hole Coulomb attraction abruptly appears. Here the hole is assumed to be localized. The Hamiltonian describing the electron–hole correlation is given by $\hat{\mathcal{H}}^{\rm h}_{\rm int}(s) = \hat{\mathcal{H}}^{\rm h}_{\rho} + \hat{\mathcal{H}}^{\rm h}_{\sigma}(s)$ with [70]

$$\mathcal{H}^{\rm h}_{\rho} = -\frac{g^{\rm h}_{2\rho}}{2}\left(\frac{\pi K_{\rho}}{L}\right)^{1/2}\sum_{p>0}\sqrt{p}\left(\hat{\alpha}^{\dagger}_{\rho p} + \hat{\alpha}_{\rho p} + \hat{\beta}^{\dagger}_{\rho p} + \hat{\beta}_{\rho p}\right), \tag{46}$$

$$\mathcal{H}^{\rm h}_{\sigma}(s) = -\frac{g^{\rm h}_{2\sigma}}{2}\left(\frac{\pi K_{\sigma}}{L}\right)^{1/2} s\sum_{p>0}\sqrt{p}\left(\hat{\alpha}^{\dagger}_{\sigma p} + \hat{\alpha}_{\sigma p} + \hat{\beta}^{\dagger}_{\sigma p} + \hat{\beta}_{\sigma p}\right), \tag{47}$$

where $g^{\rm h}_{2\rho} = (g^{\rm h}_{2\parallel} + g^{\rm h}_{2\perp})/2$ and $g^{\rm h}_{2\sigma} = (g^{\rm h}_{2\parallel} - g^{\rm h}_{2\perp})/2$ denote the strength of the electron–hole forward scattering. Using this electron–hole interaction, we calculate the single-hole Green function of the TL liquid in time domain; $G^{\rm h}_{\rm s}(t) \equiv -{\rm i}\Theta(t){\rm e}^{-{\rm i}E_0 t/\hbar}\langle {\rm e}^{{\rm i}t\hat{\mathcal{H}}^{\rm e}/\hbar}{\rm e}^{-{\rm i}t[\hat{\mathcal{H}}^{\rm e}+\hat{\mathcal{H}}^{\rm h}_{\rm int}(s)]/\hbar}\rangle \sim t^{-\beta_{\rm oc}}$, where E_0 is the energy separation between the core level and the Fermi level. Here the

critical exponent $\beta_{\rm oc}$ is independent of the hole spin and is given as

$$\beta_{\rm oc} = \frac{1}{64}\sum_{\nu=\rho,\sigma}\left(\frac{g^{\rm h}_{2\nu}}{v_{\rm F}+g_{4\nu}}\right)^2\left(K_\nu+K_\nu^{-1}\right)^4\left\{1\mp\left[1-4\left(K_\nu+K_\nu^{-1}\right)^{-2}\right]^{1/2}\right\}$$
$$= \frac{1}{4}\sum_{\nu=\rho,\sigma}\left(\frac{g^{\rm h}_{2\nu}}{v_{\rm F}+g_{4\nu}}\right)^2\left(1-\frac{g_{2\nu}}{v_{\rm F}+g_{4\nu}}\right)^{-1/2}\left(1+\frac{g_{2\nu}}{v_{\rm F}+g_{4\nu}}\right)^{-3/2}\geqslant 0, \qquad (48)$$

where $K_\nu < 1$ ($K_\nu > 1$) corresponds to the $-$ (+) sign on the right-hand side of equation (48).

An asymptotic behaviour of the core-level photoemission spectrum near the main peak, which is given by the Fourier transform of $G^{\rm h}_{\rm s}(t)$, i.e. $P_{\rm core}(\epsilon)\sim(E_{\rm core}-\epsilon)^{\beta_{\rm oc}-1}\Theta(E_{\rm core}-\epsilon)$, shows the power-law divergence near $\epsilon\sim 0$ because of $0\leqslant\beta_{\rm oc}<1$. Appearance of the power-law singularity instead of the δ-function peak means that the quasiparticle picture is invalid in the TL liquid, resulting from simultaneous excitation of many particle–vacancy pairs near the Fermi level.

8.3. The one-photon absorption: $(N, 0)\rightarrow(N+1, 1)$

We shall consider the OPA process. The absorption spectrum $W_{\rm OPA}(\omega)$ also exhibits the power-law singularity near the Fermi edge with an exponent $\beta_{\rm FES}$. The critical exponent $\beta_{\rm FES}$ is directly related to a power-law exponent of the current–current correlation function $C_s(t)$ at zero temperature: $C_s(t)=\langle {\rm e}^{{\rm i}t\hat{\mathcal{H}}^{\rm e}/\hbar}\hat{\psi}_s{\rm e}^{-{\rm i}t[\hat{\mathcal{H}}^{\rm e}+\hat{\mathcal{H}}^{\rm h}_{\rm int}(s)]/\hbar}\hat{\psi}_s^\dagger\rangle=\langle\hat{\mathcal{J}}_s^\dagger(t)\hat{\mathcal{J}}_s(0)\rangle$ with $\hat{\psi}_s\equiv\hat{\psi}_{1{\rm s}}(0)+\hat{\psi}_{2{\rm s}}(0)$. Here the current operator is $\hat{\mathcal{J}}_s(t)\equiv{\rm e}^{{\rm i}t\hat{\mathcal{H}}^{\rm e}/\hbar}\sum_{j=1,2}\hat{U}_s\hat{\psi}^\dagger_{js}{\rm e}^{-{\rm i}t\hat{\mathcal{H}}^{\rm e}/\hbar}$, where the unitary operator $\hat{U}_s$ is defined through $\hat{U}_s^\dagger\hat{\mathcal{H}}^{\rm e}\hat{U}_s=\hat{\mathcal{H}}^{\rm e}+\hat{\mathcal{H}}^{\rm h}_{\rm int}(s)$. For large t, $C_s(t)$ decays as a power law: $C_s(t)\sim t^{-\beta_{\rm FES}-1}$. Then the OPA spectrum, which is the Fourier transform of $C_s(t)$, shows the power-law anomaly, i.e. $W_{\rm OPA}(\omega)\sim(\hbar\omega-E_{\rm FES})^{\beta_{\rm FES}}\Theta(\hbar\omega-E_{\rm FES})$, where $E_{\rm FES}$ is an energy of the Fermi absorption edge.

The FES exponent consists of three parts as $\beta_{\rm FES}=\beta_{\rm TL}+\beta_{\rm oc}+\beta_{\rm ex}$ [69, 70], where $\beta_{\rm TL}$ and $\beta_{\rm oc}$ are positive (corresponding to *suppression* of the transition probability) and given by equations (45) and (48), respectively, but $\beta_{\rm ex}$ is negative, indicating the *enhancement* of the transition probability, i.e.

$$\beta_{\rm ex}=-\frac{1}{4}\sum_{\nu=\rho,\sigma}\frac{g^{\rm h}_{2\nu}}{v_{\rm F}+g_{4\nu}}\left(K_\nu+K_\nu^{-1}\right)=-\frac{1}{2}\sum_{\nu=\rho,\sigma}\frac{g^{\rm h}_{2\nu}}{v_{\rm F}+g_{4\nu}}\left[1-\left(\frac{g_{2\nu}}{v_{\rm F}+g_{4\nu}}\right)^2\right]^{-1/2}\leqslant 0, \qquad (49)$$

which is an effect due to the Mahan exciton. Thus the FES exponent in OPA spectra contains all information on the TL-liquid character ($\beta_{\rm TL}\geqslant 0$), the orthogonality catastrophe ($0\leqslant\beta_{\rm oc}<1$), and the many-body excitonic correlations ($\beta_{\rm ex}\leqslant 0$). Therefore the FES exponent can be either negative or positive depending on the balance between the positive parts $\beta_{\rm TL}+\beta_{\rm oc}$ and the negative part $\beta_{\rm ex}$. The negative (positive) $\beta_{\rm FES}$ results in the power-law divergence (convergence) of the edge spectra. The electron–hole attraction ($g^{\rm h}_{2\|}>0$ and $g^{\rm h}_{2\perp}>0$) is necessary to obtain the divergent edge. Here we note that the FES exponent of the TL liquid is independent of the hole motion [69]. These results are summarized in table 3. The FES has been observed clearly in several experiments using modulation-doped semiconductor wires [71]. Magnetic-field effects [72] and the long-range Coulomb interactions [73] have been studied extensively, but nonlinear responses of the Mahan exciton remain to be understood.

Table 3. Comparison among the critical exponents of power-law singularities in several optical spectra of a $d = 1$ metal. Corresponding correlation functions are also given. Here $\hat{\psi}$ is the field operator of an electron, $\hat{\mathcal{H}}^{\rm e}$ is the electronic Hamiltonian, and $\hat{\mathcal{H}}^{\rm h}_{\rm int}$ means the electron-core hole interaction.

Optical spectra	Critical exponents	Corresponding correlation functions
Valence-band photoemission $P_{\rm PES}(\epsilon)$ $(N,0) \to (N-1,0)$	$\beta_{\rm TL}$	Single-electron Green function $G^{\rm e}(t) \propto \langle {\rm e}^{{\rm i}t\hat{\mathcal{H}}^{\rm e}/\hbar}\hat{\psi}\,{\rm e}^{-{\rm i}t\hat{\mathcal{H}}^{\rm e}/\hbar}\hat{\psi}^{\dagger}\rangle$ $\sim t^{-\beta_{\rm TL}-1}$
Core-level photoemission $P_{\rm core}(\epsilon)$ $(N,0) \to (N,1)$	$\beta_{\rm oc} - 1$	Single-hole Green function $G^{\rm h}(t) \propto \langle {\rm e}^{{\rm i}t\hat{\mathcal{H}}^{\rm e}/\hbar}\,{\rm e}^{-{\rm i}t[\hat{\mathcal{H}}^{\rm e}+\hat{\mathcal{H}}^{\rm h}_{\rm int}]/\hbar}\rangle$ $\sim t^{-\beta_{\rm oc}}$
One-photon absorption $W_{\rm OPA}(\omega)$ $(N,0) \to (N+1,1)$	$\beta_{\rm TL} + \beta_{\rm oc} + \beta_{\rm ex}$	Current–current correlation function $C(t) \propto \langle {\rm e}^{{\rm i}t\hat{\mathcal{H}}^{\rm e}/\hbar}\hat{\psi}\,{\rm e}^{-{\rm i}t[\hat{\mathcal{H}}^{\rm e}+\hat{\mathcal{H}}^{\rm h}_{\rm int}]/\hbar}\hat{\psi}^{\dagger}\rangle$ $\sim t^{-\beta_{\rm TL}-\beta_{\rm oc}-\beta_{\rm ex}-1}$

9. Interplay between a bound state and the spin degrees of freedom in the Fermi-edge singularity

Previous theories [74–76] of the FES told us that

(i) there are two thresholds in the absorption spectrum and
(ii) as the density increases, the absolute (lowest-energy) threshold grows continuously from the 1s exciton (X) to the divergent FES, while the other step-like continuum edge develops to the convergent FES.

In recent experiments on modulation-doped semiconductor quantum wells [77–79], the bound state gives rise to not only a sharp X peak in the spectra at low densities but also to another peak below the X peak, which is assigned to a negatively charged exciton, a 'trion' (X^-). As the density increases, the X^- peak seems to evolve smoothly into the FES, while the X peak shifts to higher energy, losing its intensity, and ultimately merges with the high-energy tail of the X^- edge spectrum. Hawrylak [80] calculated numerically the optical spectra in such systems to show two absorption peaks resulting from two spin-channel effects. Here we focus on how a bound state affects the optical spectra as the carrier density varies in $d = 2$. We try to clarify whether the thresholds are divergent or convergent and to obtain an analytical formula of the critical exponents and amplitudes of these thresholds [81].

We shall consider only the optical absorption process, and start with the Mahan–Nozières-DeDominicis Hamiltonian:

$$\hat{H} = \sum_{\boldsymbol{k},\sigma} \varepsilon_{\boldsymbol{k}} \hat{c}^{\dagger}_{\boldsymbol{k},\sigma}\hat{c}_{\boldsymbol{k},\sigma} + \varepsilon_{\rm c}\hat{d}^{\dagger}\hat{d} - \sum_{\boldsymbol{k},\boldsymbol{k}',\sigma} V(\boldsymbol{k},\,\boldsymbol{k}')\hat{c}^{\dagger}_{\boldsymbol{k}',\sigma}\hat{c}_{\boldsymbol{k},\sigma}\hat{d}^{\dagger}\hat{d}, \tag{50}$$

which describes electrons in the conduction band with two-dimensional momentum $\boldsymbol{k}$ and spin $\sigma = \pm\frac{1}{2}$ (created by $\hat{c}^{\dagger}_{k,\sigma}$) interacting with a valence-band hole ($\hat{d}^{\dagger}$) via the Coulomb interaction $V(\boldsymbol{k},\boldsymbol{k}')$. The conduction-band electrons are assumed to be noninteracting. The valence-band hole is assumed to be localized at the origin and its spin index is omitted since it plays no role in our problem; we consider only the case where the photon is σ^- polarized and a spin-up electron is excited leaving behind a hole with down spin. The system is assumed to be initially in the ground state of conduction-band electrons and a vacuum of a hole at zero temperature, denoted as $|{\rm i}\rangle$. Then the absorption spectrum can be

written as $I(\omega) = 2\,\mathrm{Re}\int_0^\infty \mathrm{d}t\,\exp(\mathrm{i}\omega t)I(t)$, where $I(t)$ is the absorption response function: $I(t) = \sum_{b,b'} w_b w_{b'} \mathcal{F}(\boldsymbol{b}, \boldsymbol{b}'|t)$ with $\mathcal{F}(\boldsymbol{b}, \boldsymbol{b}'|t) = \langle \mathrm{i}|\exp(\mathrm{i}\hat{H}t)\hat{d}\hat{c}_{b,\uparrow}\exp(-\mathrm{i}\hat{H}t)\hat{c}^\dagger_{b',\uparrow}\hat{d}^\dagger|\mathrm{i}\rangle$. Here w_b is the dipole transition matrix element at the wavevector $\boldsymbol{b}$.

In the absence of bound states, the absorption spectrum consists of one continuous spectrum that begins at the absolute threshold. Effects of electron-spin degeneracy have been thought to appear simply as follows:

(i) doubling the ground-state energy shift between the initial and a final configuration, and
(ii) changing the critical exponent tending to suppress the divergent singularity.

On the other hand, in the presence of a bound state, the final-state configuration falls into four classes depending on whether the bound states are occupied or not. In the spinless case the final-state configuration has only two classes, occupied or not. Each of these four configurations gives rise to their own spectrum starting at each threshold.

With the use of the Fermi-golden-rule approach, we find that the absorption response function, $I(t)$, has the form of

$$I(t) = \left\{\mathcal{I}_{\mathrm{X}^-}(t) + \left[\mathcal{I}^{(1)}_{\mathrm{X}}(t) + \mathcal{I}^{(2)}_{\mathrm{X}}(t)\right]\exp[-\mathrm{i}(E_\mathrm{F} + E_\mathrm{b})t] + \mathcal{I}_\mathrm{C}(t)\exp[-2\mathrm{i}(E_\mathrm{F} + E_\mathrm{b})t]\right\}\exp(-\mathrm{i}\omega_\mathrm{th}t), \tag{51}$$

where E_F is the Fermi energy measured from the bottom of the scattering states, and E_b is the energy gap between the bottom of the scattering states and the bound state (i.e. the exciton binding energy). Here the energy of the absolute threshold is $\omega_\mathrm{th} = \Delta E + E_\mathrm{F} + E_\mathrm{gap}$, where E_gap is the band-gap energy and ΔE is the ground-state energy shift due to the valence-hole potential: $\Delta E = -2\int_0^{E_\mathrm{F}} \mathrm{d}\varepsilon\,\delta(\varepsilon)/\pi - 2E_\mathrm{b}$ with the scattering phase shift $\delta(\varepsilon)$. The detailed form of $\mathcal{I}_\nu(t)$ ($\nu = \mathrm{X}^-, \mathrm{X}^{(1)}, \mathrm{X}^{(2)}$ and C) is not shown here.

The function $\mathcal{I}_{\mathrm{X}^-}(t)$, related to the spectrum beginning at the absolute threshold, results from the doubly occupied bound state (the X^- configuration in the low-density limit), and when the carrier density goes to zero ($E_\mathrm{F} \sim 0$), this threshold becomes the X^- peak. The second term, $\mathcal{I}^{(1)}_\mathrm{X}(t) + \mathcal{I}^{(2)}_\mathrm{X}(t)$, corresponds to the 'exciton' (X) in the limit of $E_\mathrm{F} \to 0$; here $\mathrm{X}^{(1)}$ ($\mathrm{X}^{(2)}$) is a spin-singlet (spin-triplet) 'exciton' in the low-density limit. The last term, $\mathcal{I}_\mathrm{C}(t)$, stands for the vacant bound state. The energy of these thresholds, $\mathcal{I}_{\mathrm{X}^-}$, $\mathcal{I}_\mathrm{X}$, and $\mathcal{I}_\mathrm{C}$, is evaluated in terms of the phase shift, respectively, as

$$\omega_{\mathrm{X}^-} = \omega_\mathrm{th} = -2\int_0^{E_\mathrm{F}} \mathrm{d}\varepsilon\frac{\delta(\varepsilon)}{\pi} - 2E_\mathrm{b} + E_\mathrm{F} + E_\mathrm{gap}, \tag{52}$$

$$\omega_\mathrm{X} \equiv \omega^{(1)}_\mathrm{X} = \omega^{(2)}_\mathrm{X} = -2\int_0^{E_\mathrm{F}} \mathrm{d}\varepsilon\frac{\delta(\varepsilon)}{\pi} - E_\mathrm{b} + 2E_\mathrm{F} + E_\mathrm{gap}, \tag{53}$$

$$\omega_\mathrm{C} = -2\int_0^{E_\mathrm{F}} \mathrm{d}\varepsilon\frac{\delta(\varepsilon)}{\pi} + 3E_\mathrm{F} + E_\mathrm{gap}. \tag{54}$$

The integrated intensity of each contribution, $\mathcal{I}_\nu(t = 0)$, is also evaluated, which will be reported elsewhere. When no spin degrees of freedom are taken into account, there are only two thresholds, 'main' (m) and 'secondary' (s). The absorption response function becomes $I_\mathrm{spinless}(t) = \{\mathcal{I}_\mathrm{m}(t) + \mathcal{I}_\mathrm{s}(t)\exp[-\mathrm{i}(E_\mathrm{F} + E_\mathrm{b})t]\}\exp(-\mathrm{i}\omega^0_\mathrm{th}t)$, where energies of the thresholds are $\omega_\mathrm{m} = \omega^0_\mathrm{th} = \frac{1}{2}\Delta E + E_\mathrm{F} + E_\mathrm{gap}$ and $\omega_\mathrm{s} = \frac{1}{2}\Delta E + E_\mathrm{b} + 2E_\mathrm{F} + E_\mathrm{gap}$.

We here present numerical results of the absorption spectra. To proceed with the numerical calculation, we employ the time-dependent coupled-cluster expansion method [82]. After the photoexcitation, the Hamiltonian becomes $\hat{H}_\mathrm{final} = \sum_{k,k',\sigma}\langle\phi_{k'}|\hat{h}|\phi_k\rangle\hat{c}^\dagger_{k',\sigma}\hat{c}_{k,\sigma} + \varepsilon_\mathrm{c}$, which is a sum of the matrix elements of electronic one-body Hamiltonians, $\langle\phi_{k'}|\hat{h}|\phi_k\rangle =$

$\delta_{k,k'}\varepsilon_k - V(\boldsymbol{k},\boldsymbol{k}')$. Then we have an integrodifferential equation for $\mathcal{F}(\boldsymbol{b},\boldsymbol{b}'|t)$ in a closed form:

$$\mathrm{i}\frac{\mathrm{d}}{\mathrm{d}t}\mathcal{F}(\boldsymbol{b},\boldsymbol{b}'|t) = [\varepsilon_{\mathrm{c}} - 2\eta(t)]\mathcal{F}(\boldsymbol{b},\boldsymbol{b}'|t) + \sum_{\boldsymbol{b}''(>)}\left[\langle\phi_{\boldsymbol{b}}|\hat{h}|\phi_{\boldsymbol{b}''}\rangle - \sum_{\boldsymbol{m}(<)} s(\boldsymbol{b},\boldsymbol{m}|t)\langle\phi_{\boldsymbol{m}}|\hat{h}|\phi_{\boldsymbol{b}''}\rangle\right]\mathcal{F}(\boldsymbol{b}'',\boldsymbol{b}'|t), \tag{55}$$

where

$$\eta(t) = -\sum_{\boldsymbol{m}(<)}\left[\langle\phi_{\boldsymbol{m}}|\hat{h}|\phi_{\boldsymbol{m}}\rangle - \varepsilon_{\boldsymbol{m}}\right] - \sum_{\boldsymbol{b}(>)}\sum_{\boldsymbol{m}(<)} s(\boldsymbol{b},\boldsymbol{m}|t)\langle\phi_{\boldsymbol{m}}|\hat{h}|\phi_{\boldsymbol{b}}\rangle, \tag{56}$$

$$\mathrm{i}\frac{\mathrm{d}}{\mathrm{d}t}s(\boldsymbol{b},\boldsymbol{m}|t) = \langle\phi_{\boldsymbol{b}}|\hat{h}|\phi_{\boldsymbol{m}}\rangle + \sum_{\boldsymbol{b}'(>)}\langle\phi_{\boldsymbol{b}}|\hat{h}|\phi_{\boldsymbol{b}'}\rangle s(\boldsymbol{b}',\boldsymbol{m}|t) - \sum_{\boldsymbol{m}'(<)} s(\boldsymbol{b},\boldsymbol{m}'|t)\langle\phi_{\boldsymbol{m}'}|\hat{h}|\phi_{\boldsymbol{m}}\rangle - \sum_{\boldsymbol{b}'(>)}\sum_{\boldsymbol{m}'(<)} s(\boldsymbol{b},\boldsymbol{m}'|t)\langle\phi_{\boldsymbol{m}'}|\hat{h}|\phi_{\boldsymbol{b}'}\rangle s(\boldsymbol{b}',\boldsymbol{m}|t). \tag{57}$$

The symbol $<$ ($>$) in the summations means 'below' ('above') the Fermi level. The initial conditions are given by $\mathcal{F}(\boldsymbol{b},\boldsymbol{b}'|0) = \delta_{\boldsymbol{b},\boldsymbol{b}'}$ and $s(\boldsymbol{b},\boldsymbol{m}|0) = 0$.

For simplicity, the valence-hole potential is assumed to be a contact-type V. We take the centre of the conduction band as the origin $\varepsilon = 0$ of the energy level and the unit of energy is a half of the total band width of the conduction band. Then the Fermi energy ε_{F} is in a range of $-1 \leqslant \varepsilon_{\mathrm{F}} \leqslant 1$. The density of states of the conduction band in $d = 2$ is constant: $N(\varepsilon) = \frac{1}{2}$ for $-1 \leqslant \varepsilon \leqslant 1$. The energy level of a bound state is $\varepsilon_\lambda = -\coth(1/V)$. The phase shift $\delta(\varepsilon)$ is calculated as $\tan\delta(\varepsilon) = \pi V\left[2 + V\log|(1+\varepsilon)/(1-\varepsilon)|\right]^{-1}$ for two-dimensional systems.

Figure 2 shows typical absorption spectra in $d = 2$ for several values of the Fermi energy ε_{F}. We see a symmetric X peak and a broad continuum band, and no sign of the X^- threshold appears in the insulator limit ($\varepsilon_{\mathrm{F}} = -1$). As the Fermi energy increases, we can see an abrupt increase of the $\mathcal{I}_{\mathrm{X}^-}$ intensity and decrease of $\mathcal{I}_{\mathrm{X}}$ and $\mathcal{I}_{\mathrm{C}}$. At finite ε_{F}, $\mathcal{I}_{\mathrm{X}^-}$ and $\mathcal{I}_{\mathrm{X}}^{(1)}$ become divergent power-law singularities. For comparison, absorption spectra calculated with the spinless fermion theory are also shown, which have only two thresholds.

In the long-time limit, the functions $\mathcal{I}_\nu(t)$ exhibit a power-law decay. Then near the threshold region, the spectra behave asymptotically as $I_\nu(\omega) \propto \mu_\nu\,(\omega - \omega_\nu)^{\beta_\nu}$. The critical exponents β_ν are

$$\beta_{\mathrm{X}^-} = (\delta_0/\pi - 1)^2 + (\delta_0/\pi)^2 - 1 \leqslant 0, \tag{58}$$

$$\beta_{\mathrm{X}}^{(1)} = 2(\delta_0/\pi - 1)^2 - 1, \tag{59}$$

$$\beta_{\mathrm{X}}^{(2)} = (\delta_0/\pi - 2)^2 + (\delta_0/\pi)^2 - 1 > 0, \tag{60}$$

$$\beta_{\mathrm{C}} = (\delta_0/\pi - 2)^2 + (\delta_0/\pi - 1)^2 - 1 \geqslant 0, \tag{61}$$

with the phase shift at the Fermi level, $\delta_0 = \delta(\varepsilon = \varepsilon_{\mathrm{F}})$. These critical exponents satisfy Hopfield's rule of thumb. The critical amplitudes μ_ν are also analytically obtained but are very complicated, and will be given elsewhere. When no spin degrees of freedom are taken into account, the exponents of the thresholds are $\beta_{\mathrm{m}} = (\delta_0/\pi - 1)^2 - 1 \leqslant 0$ and $\beta_{\mathrm{s}} = (\delta_0/\pi - 2)^2 - 1 \geqslant 0$.

The absolute (lowest) threshold (X^-) is always divergent since $\beta_{\mathrm{X}^-} \leqslant 0$, while the C (highest) threshold is always convergent ($\beta_{\mathrm{C}} \geqslant 0$). At the X threshold the first contribution $\mathcal{I}_{\mathrm{X}}^{(1)}(\omega)$ leads to a divergent threshold only when $\delta_0/\pi > 1 - 1/\sqrt{2}$, whereas the second

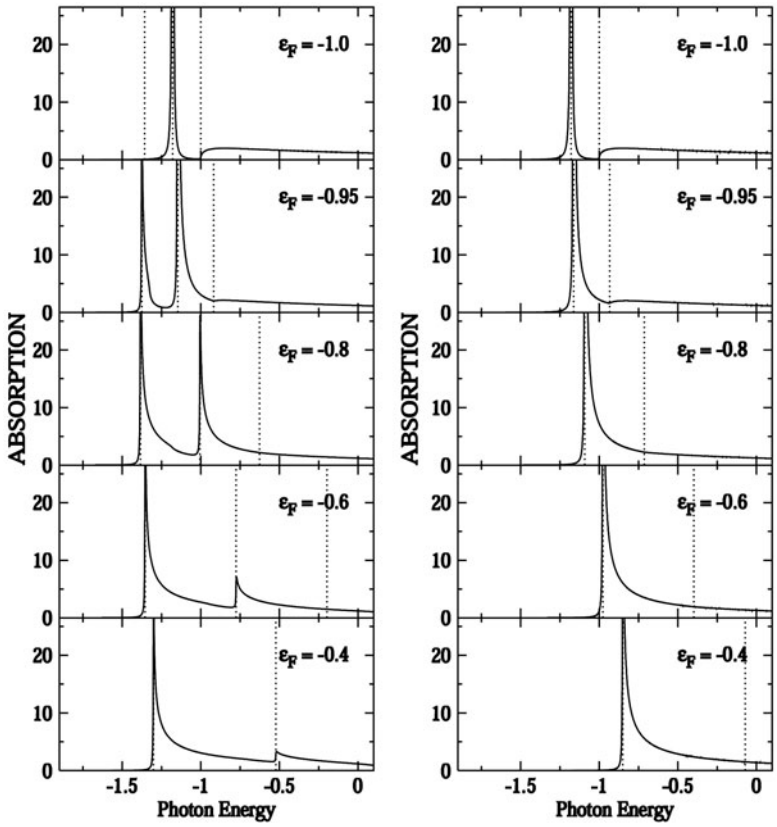

Figure 2. Optical absorption spectra in $d = 2$ for the contact-type hole potential $V = 0.8$, where the exciton binding energy is $E_b = 0.179$. The left (right) column corresponds to the case where the spin degrees of freedom are (are not) taken into account. The Fermi level ε_F is chosen to be -1.0 (undoped case), -0.95, -0.8, -0.6 and -0.4 from top to bottom. In the left column, the three dashed vertical lines represent the threshold energies of the doubly occupied (ω_{X^-}), singly occupied (ω_X) and vacant bound states (ω_C), respectively. (For $\varepsilon_F = -0.4$, ω_C is out of range.) In the right column, there are only two threshold energies, ω_m and ω_s. A phenomenological dephasing constant is chosen to be 0.002.

one $\mathcal{I}_X^{(2)}(\omega)$ is always convergent. In the low-doping limit, δ_0 approaches π from below, then $\mathcal{I}_X^{(1)}(\omega)$ tends to a δ-function-like absorption line, the X peak. We note that the exponent $\beta_X^{(1)}$ is a monotonously increasing function of δ_0. As the Fermi energy (the doping density) is increased, the exponent $\beta_X^{(1)}$ increases from $\beta_X^{(1)} < 0$ to $\beta_X^{(1)} > 0$, hence $\beta_X^{(1)}$ changes its sign. Therefore, the $X^{(1)}$ threshold exhibits the crossover from the divergent to the convergent edge spectrum. This is a characteristic peculiar to the spin-$\frac{1}{2}$ model. We note that the photoluminescence spectra in $d = 1$ and 2 have also been calculated.

On-site Coulomb repulsion between two bound-state electrons is not included in the present theory. This leads to a major quantitative difference from the experimental results. Moreover we take the strength of the valence-hole potential V as a parameter independent of the carrier density. In actual systems, however, the potential $V(\boldsymbol{k}, \boldsymbol{k}')$ will not be a contact type and may depend on the carrier density. Spin-dependent, exchange-type interactions should also be incorporated. Not only such electronic correlation but also effects of motion of a hole are left for future studies.

10. Conclusions

We have overviewed several exciton-related problems from theoretical viewpoints. In particular, we stress universal (material-independent) features of low-dimensional exciton systems. One notices the crucial importance of the dimensionality of materials in optical responses of meso- and microscopic systems. Geometrical confinement of excitons and the dielectric image-charge effects as well as the single-electron band structures are keys for designing novel materials with new optical functions. Moreover, many-body effects, electron–electron correlations, the Fermi-surface effects and the quantum fluctuations also play important roles in the optical responses of low-dimensional materials.

All the exciton problems attracting interest recently are related to quantum many-body problems and/or to nonequilibrium dynamics far from thermal equilibrium. Not only the electron, the hole and the mutual Coulomb interaction, but also their stage and some supporting players, contribute to novel properties. For example, the exciton-lattice interactions lead to the self-trapping phenomena [83], the randomness can induce exciton weak localization [84], or exciton–photon interaction results in exciton squeezing. These effects and their dimensionality open new fields in photophysics. Moreover, it will be of great interest to use photons not only as a probe for materials but also as a trigger for drastic change and control of the material states, even including the ground state. This photoinduced phase transition [85] is also a new, promising field, where details of excited states should be well understood.

Although the theories introduced here do not always include all the actual details, we believe that these findings hold universally in electron–hole systems and will be of great significance in the interpretation of experimental results. In addition, this paper will offer a guiding principle in the materials design of new low-dimensional materials.

Acknowledgments

These works presented in this paper have been supported by PRESTO and CREST, JST and by the Grant-in-Aids from the Ministry of Education, Culture, Sports, Science and Technology of Japan.

References

[1] Ogawa T and Kanemitsu Y 1995 and 1998 *Optical Properties of Low-Dimensional Materials* vol 1 and 2 (Singapore: World Scientific)
[2] Ogawa T 1997 *Nonlinear Opt.* **18** 181
[3] This article does not treat quasi-zero-dimensional ($d \simeq 0$) semiconductors, 'quantum dots'. See, e.g. Bányai L and Koch S W 1993 *Semiconductor Quantum Dots* (Singapore: World Scientific)
Jacak L, Hawrylak P and Wójs A 1998 *Quantum Dots* (Berlin: Springer)
Masumoto Y and Takagahara T (ed) 2002 *Semiconductor Quantum Dots* (Berlin: Springer)
[4] Shinada M and Sugano S 1966 *J. Phys. Soc. Japan* **21** 1936
[5] Shinozuka Y and Matsuura M 1983 *Phys. Rev.* B **28** 4878
Shinozuka Y and Matsuura M 1984 *Phys. Rev.* B **29** 3717 (erratum)
[6] Loudon R 1959 *Am. J. Phys.* **27** 649
Elliot R J and Loudon R 1959 *J. Phys. Chem. Solids* **8** 382
Elliot R J and Loudon R 1960 *J. Phys. Chem. Solids* **15** 196
Abe S 1989 *J. Phys. Soc. Japan* **58** 62
[7] Ogawa T and Takagahara T 1991 *Phys. Rev.* B **43** 14325
[8] Bányai L, Galbraith I, Ell C and Haug H 1987 *Phys. Rev.* B **36** 6099
[9] Ogawa T and Takagahara T 1991 *Phys. Rev.* B **44** 8138
Ogawa T and Takagahara T 1992 *Surf. Sci.* **263** 506
[10] Ogawa T 1994 *Light Emission from Novel Silicon Materials* (Tokyo: Phys. Soc. Jpn.) p 120

[11] Low-dimensional excitonic effects have been discussed in relation to luminescence processes of silicon nanocrystals. See, e.g. Ohno T, Shiraishi K and Ogawa T 1992 *Phys. Rev. Lett.* **69** 2400
Kanemitsu Y, Ogawa T, Shiraishi K and Takeda K 1993 *Phys. Rev.* B **48** 4883
[12] Ando H, Oohashi H and Kanbe H 1991 *J. Appl. Phys.* **70** 7024
[13] Akiyama H, Pfeiffer L N, Yoshita M, Pinczuk A and West K W 2003 *Appl. Phys. Lett.* **82** 379
[14] Itoh H, Hayamizu Y, Yoshita M, Akiyama H, Pfeiffer L N, West K W, Szymanska M H and Littlewood P B 2003 *Appl. Phys. Lett.* **83** 2043
[15] Mahan G D 1968 *Phys. Rev.* **170** 825
[16] Shimizu A 1989 *Phys. Rev.* B **40** 1403
[17] Shimizu A, Ogawa T and Sakaki H 1992 *Phys. Rev.* B **45** 11338
Shimizu A, Ogawa T and Sakaki H 1992 *Surf. Sci.* **263** 512
[18] Ogawa T and Shimizu A 1993 *Phys. Rev.* B **48** 4910
[19] Cingolani R, Lepore M, Tommasi R, Catalano I M, Lage H, Heitmann D, Ploog K, Shimizu A, Sakaki H and Ogawa T 1992 *Phys. Rev. Lett.* **69** 1276
Cingolani R, Lepore M, Tommasi R, Catalano I M, Lage H, Heitmann D, Ploog K, Shimizu A, Sakaki H and Ogawa T 1993 *Superlatt. Microstruct.* **13** 71
[20] Rinaldi R, Cingolani R, Lepore M, Ferrara M, Catalano I M, Rossi F, Rota L, Molinari E, Lugli P, Marti U, Martin D, Morier-Gemoud F, Ruterana P and Reinhart F K 1994 *Phys. Rev. Lett.* **73** 2899
[21] Keldysh L V 1979 *JETP Lett.* **29** 658
Keldysh L V 1988 *Superlatt. Microstruct.* **4** 637
[22] Hanamura E, Nagaosa N, Kumagai M and Takagahara T 1988 *Mater. Sci. Eng.* B **1** 255
[23] Kleinman D A 1983 *Phys. Rev.* B **28** 871
[24] Akimoto O and Hanamura E 1972 *J. Phys. Soc. Japan* **33** 1537
[25] Ishida K, Aoki H and Ogawa T 1995 *Phys. Rev.* B **52** 8980
[26] Kuwata-Gonokami M, Peyghambarian N, Meissner K, Fluegel B, Sato Y, Ema K, Shimano K, Mazumdar S, Guo F, Tokihiro T, Ezaki H and Hanamura E 1994 *Nature* **367** 47
[27] Stébé B, Munschy G, Stauffer L, Dujardin F and Murat J 1997 *Phys. Rev.* B **56** 12454
Kheng K, Cox R T, Merle d'Aubigne Y, Bassani F, Saminadayar K and Tatarenko S 1993 *Phys. Rev. Lett.* **71** 1752
[28] Nasu K (ed) 1997 *Relaxations of Excited States and Photo-Induced Phase Transitions* (Berlin: Springer)
[29] Koshino K and Ogawa T 1998 *Phys. Rev.* B **58** 14804
Koshino K and Ogawa T 1998 *J. Phys. Soc. Japan* **67** 2174
[30] Östreich Th, Schönhammer K and Sham L J 1995 *Phys. Rev. Lett.* **74** 4698
Combescot M and Combescot R 1988 *Phys. Rev. Lett.* **61** 117
[31] Haug H and Koch S W 1994 *Quantum Theory of the Optical and Electronic Properties of Semiconductors* 4th edn (Singapore: World Scientific)
[32] Lindberg M and Koch S W 1988 *Phys. Rev.* B **38** 3342
[33] Ivanov A L, Haug H and Keldysh L V 1998 *Phys. Rep.* **296** 237
[34] Axt V M, Bartels G and Stahl A 1996 *Phys. Rev. Lett.* **76** 2543
The excitation-induced dephasing was considered in the semiconductor Bloch equations to treat the $\chi^{(3)}$ process
Lindberg M, Hu Y Z, Binder R and Koch S W 1994 *Phys. Rev.* B **50** 18060
[35] Axt V M and Stahl A 1994 *Z. Phys.* B **93** 195
Axt V M and Mukamel S 1998 *Rev. Mod. Phys.* **70** 145
Pereira M F and Henneberger K 1998 *Phys. Rev.* B **58** 2064
[36] Kuwata-Gonokami M, Inouye S, Suzuura H, Shirane M, Shimano R, Someya T and Sakaki H 1997 *Phys. Rev. Lett.* **79** 1341
[37] Hanamura E and Haug H 1977 *Phys. Rep.* **33** 209
[38] Fukuzawa T, Kano S S, Gustafson T K and Ogawa T 1990 *Surf. Sci.* **228** 482
[39] Hiroshima T 1989 *Phys. Rev.* B **40** 3862
[40] Inoue J, Brandes T and Shimizu A 1998 *J. Phys. Soc. Japan* **67** 3384
[41] Takayama R, Kwong N H, Rumyantsev I, Kuwata-Gonokami M and Binder R 2002 *Eur. Phys. J.* B **25** 445
[42] Combescot M and Betbeder-Matibet O 2002 *Europhys. Lett.* **58** 87
Betbeder-Matibet O and Combescot M 2002 *Eur. Phys. J.* B **27** 505
[43] Usui T 1960 *Prog. Theor. Phys.* **23** 787
[44] Hawton M and Nelson D 1998 *Phys. Rev.* B **57** 4000
[45] Marumori T, Yamamura M and Tokunaga A 1964 *Prog. Theor. Phys.* **31** 1009
[46] Kishimoto T and Tamura T 1983 *Phys. Rev.* C **27** 341
[47] Iachello F and Arima A 1987 *The Interacting Boson Model* (Cambridge: Cambridge University Press)

Talmi I 1993 *Simple Models of Complex Nuclei* (New York: Harwood Academic)
[48] Okumura S and Ogawa T 2002 *Phys. Rev.* B **65** 035105
[49] Okumura S and Ogawa T 2002 *Nonlinear Opt.* **29** 571
[50] Kopietz P 1997 *Bosonization of Interacting Fermions in Arbitrary Dimensions* (Berlin: Springer)
[51] Gogolin A O, Nersesyan A A and Tsvelik A M 1998 *Bosonization and Strongly Correlated Systems* (Cambridge: Cambridge University Press)
[52] Mahan G D 2000 *Many-Particle Physics* 3rd edn (New York: Plenum)
[53] Tomonaga S 1950 *Prog. Theor. Phys.* **5** 544
Luttinger J M 1963 *J. Math. Phys.* **4** 1154
Haldane F D M 1980 *Phys. Rev. Lett.* **45** 1358
Solyom J 1979 *Adv. Phys.* **28** 201
[54] Nozieres P and Schmitt-Rink S 1985 *J. Low. Temp. Phys.* **59** 195
[55] Ivanov A L and Haug H 1993 *Phys. Rev. Lett.* **71** 3182
[56] Tanguy C and Combescot M 1992 *Phys. Rev. Lett.* **68** 1935
Foing J-P, Hulin D, Joffre M, Jackson M K, Oudar J-L, Tanguy C and Combescot M 1992 *Phys. Rev. Lett.* **68** 110
[57] Nagaosa N and Ogawa T 1993 *Solid State Commun.* **88** 295
[58] Asano K and Ogawa T 2005 *J. Lumin.* at press
[59] Ogawa T 1995 *Phys. Status Solidi* b **188** 83
[60] Nagai M, Shimano R and Kuwata-Gonokami M 2001 *Phys. Rev. Lett.* **86** 5795
[61] Shimano R, Nagai M, Horiuchi K and Kuwata-Gonokami M 2002 *Phys. Rev. Lett.* **88** 057404
[62] Ishikawa A, Ogawa T and Sugakov V I 2001 *Phys. Rev.* B **64** 144301
[63] Sugakov V I 1998 *Solid State Commun.* **106** 705
[64] Nazarenko A V, Ogawa T and Sugakov V I 2001 *Phys. Status Solidi* b **228** 857
[65] Ishikawa A and Ogawa T 2002 *Phys. Rev.* E **65** 026131
[66] Ogawa T and Ishikawa A 2004 *J. Lumin.* **108** 263
[67] Kondo J and Yoshimori A (ed) 1988 *Fermi Surface Effects* (Berlin: Springer)
[68] Ohtaka K and Tanabe Y 1990 *Rev. Mod. Phys.* **62** 929
[69] Ogawa T, Furusaki A and Nagaosa N 1992 *Phys. Rev. Lett.* **68** 3638
[70] Ogawa T 1997 *Mater. Sci. Eng.* B **48** 131
Ogawa T 1998 *Physica* B **249** 185
[71] Calleja J M, Goni A R, Dennis B S, Weiner J S, Pinczuk A, Schmitt-Rink S, Pfeiffer L N, West K W, Muller J F and Ruckenstein A E 1991 *Solid State Commun.* **79** 911
For a $d \simeq 2$ system, see Skolnick M S, Rorison J M, Nash K J, Mowbray D J, Tapster P R, Bass S J and Pitt A D 1987 *Phys. Rev. Lett.* **58** 2130
[72] Ogawa T and Otani H 1995 *J. Phys. Soc. Japan* **64** 3664
Otani H and Ogawa T 1996 *Phys. Rev.* B **53** 4684
[73] Otani H and Ogawa T 1996 *Phys. Rev.* B **54** 4540
[74] Combescot M and Nozières P 1971 *J. Physique* **32** 913
[75] Tanabe Y and Ohtaka K 1984 *Phys. Rev.* B **29** 1653
[76] Ruceknstein A E and Schmitt-Rink S 1987 *Phys. Rev.* B **35** 7551
[77] Huard V, Cox R T, Saminadayar K, Arnoult A and Tatarenko S 2000 *Phys. Rev. Lett.* **84** 187
[78] Yusa G, Shtrikman H and Bar-Joseph I 2000 *Phys. Rev.* B **62** 15390
[79] Brown S A, Young J F, Brum J A, Hawrylak P and Wasilewski Z 1996 *Phys. Rev.* B **54** R11082
[80] Hawrylak P 1991 *Phys. Rev.* B **44** 3821
[81] Takagiwa M and Ogawa T 2002 *J. Phys. Chem. Solids* **63** 1587
[82] Primozich N, Shahbazyan T V and Perakis I E 2000 *Phys. Rev.* B **61** 2041
[83] Sumi H and Sumi A 1994 *J. Phys. Soc. Japan* **63** 637
[84] Hanamura E 1996 *Phys. Rev.* B **54** 11219
[85] Nasu K, Tanimura K, Ogawa T and Nakamura A (ed) 2002 *Photoinduced Phase Transitions, Their Dynamics and Precursor Phenomena, Phase Transitions* vol 75 (London: Taylor and Francis)